PALEOCEANOGRAPHY, VOL. 9, NO. 4, PAGES 559-578, AUGUST 1994

Beryllium 10, thorium 230, and protactinium 231 in Galapagos microplate sediments: Implications of hydrothermal activity and paleoproductivity changes during the last 100,000 years

Martin Frank,[1] Jörg-Detlef Eckhardt,[2] Anton Eisenhauer,[1] Peter W. Kubik,[3] Beate Dittrich-Hannen,[3] Monika Segl,[4] and Augusto Mangini[1]

Abstract. Biogenic particle fluxes from highly productive surface waters, boundary scavenging, and hydrothermal activity are the main factors influencing the deposition of radionuclides in the area of the Galapagos microplate, eastern Equatorial Pacific. In order to evaluate the importance of these three processes throughout the last 100 kyr, concentrations of the radionuclides ^{10}Be, ^{230}Th, and ^{231}Pa, and of Mn and Fe were measured at high resolution in sediment samples from two gravity cores KLH 068 and KLH 093. High biological productivity in the surface waters overlying the investigated area has led to ^{10}Be and ^{231}Pa fluxes exceeding production during at least the last 30 kyr and probably the last 100 kyr. However, during periods of high productivity at the upwelling centers off Peru and extension of the equatorial high-productivity zone, a relative loss of ^{10}Be and ^{231}Pa may have occurred in these sediment cores because of boundary scavenging. The effects of hydrothermal activity were investigated by comparing the ^{230}Th$_{ex}$ concentrations to the Mn/Fe ratios and by comparing the fluxes of ^{230}Th and ^{10}Be which exceed production. The results suggest an enhanced hydrothermal influence during isotope stages 4 and 5 and to a lesser extent during isotope stage 1 in core KLH 093. During isotope stages 2 and 3, the hydrothermal supply of Mn was deposited elsewhere, probably because of changes in current regime or deepwater oxygenation. A strong increase of the Mn/Fe ratio at the beginning of climatic stage 1 which is not accompanied by an increase of the ^{230}Th$_{ex}$ concentration is interpreted to be an effect of Mn remobilization and reprecipitation in the sediment.

Introduction

The radionuclides ^{10}Be, ^{230}Th, and ^{231}Pa have been used for dating sediments and for tracing geochemical and sedimentological phenomena for more than two decades. Beryllium 10 ($T_{1/2}$ = 1.52 Ma [*Hofmann et al.*, 1987]) is produced in the upper atmosphere by cosmic radiation depending on the geographical latitude [*Lal and Peters*, 1967] and is then transferred to the Earth's surface by wet and dry precipitation with a residence time in the atmosphere of about 1 year [c.f. *Turekian et al.*, 1983]. The present global average production was calculated to be $1.21 \pm 0.26 \cdot 10^6$ atoms/cm^{2}yr [*Monaghan et al.*, 1985/1986]. This production rate is influenced by variations of the geomagnetic field intensity [*Henken-Mellies et al.*, 1990], and there are indications that during the last glacial maximum, there was a 30 % increase of the production of ^{10}Be [*Lao et al.*, 1992a]. This was also considered to be the maximum range of variation during the last about 420 kyr, as suggested by *Southon et al.* [1987]. However, there are detailed investigations of the production rate variations of ^{14}C during the last 50 kyr which show an increase of the production in the period from 15 to 24 kyr and from 37 to 46 kyr B.P. of up to 90 % above the present-day value [*Mazaud et al.*, 1991]. There is evidence that the production of ^{10}Be varied to the same extent. Having reached the oceans, ^{10}Be is quickly adsorbed to particles, preferably aluminosilicates [*Sharma et al.*, 1987]. The biological activity in the surface waters of the ocean produces bigger particles (e.g., fecal pellets) incorporating the clay minerals. The bigger particles have a high sinking velocity and redissolve in the deeper water column. This explains the nutrient-like behavior of ^{10}Be in ocean water column profiles [*Kusakabe et al.*, 1987].

However, there are still uncertainties concerning the ^{10}Be adsorber phases, as recently shown by *Lao et al.* [1993], who did not find a relationship between Al and ^{10}Be in sediment trap samples from off the west coast of the United

[1] Heidelberger Akademie der Wissenschaften, Heidelberg, Germany.
[2] Institut für Petrographie und Geochemie, Universität Karlsruhe, Karlsruhe, Germany.
[3] Institut für Teilchenphysik der Eidgenössisch Technischen Hochschule Zürich, Zürich, Switzerland.
[4] Fachbereich Geowissenschaften, Universität Bremen, Bremen, Germany.

Paper number 94PA01132.
0883-8305/94/94PA-01132$10.00

States. It is proposed that in such a high particle flux area, biogenic opal may be a more important scavenging factor than clay [*Lao et al.*, 1992c, 1993]. This was also deduced by *Bourlès et al.* [1989a] from sequential leaching experiments of natural sediments and by *Bourlès et al.* [1989b] from the comparison of Be and Si in pore water profiles.

Fe oxihydroxides which are the products of the oxidation of Fe sulfides emanated by hydrothermal activity may be another scavenging factor for ^{10}Be in the direct neighbourhood of mid-ocean ridges [*Valette-Silver et al.*, 1987; *Bourlès et al.*, 1991]. According to *Anderson et al.* [1990], Mn, for example, released to the bottom water by diagenetic recycling does not scavenge ^{10}Be to a remarkable amount. However, *Bourlès et al.* [1989a] found a relationship between ^{10}Be and Mn, and Fe oxihydroxides in sequential leaching experiments of various sediments and a relationship between Mn and Be in pore waters of the hydrothermally influenced sedimentary environment of the Guayamas Basin [*Bourlès et al.*, 1989b]. Nevertheless the affinity of Be for adsorbing to oxihydroxides should be less compared to ^{230}Th and ^{231}Pa, as the results of *Anderson et al.* [1990] and *Lao et al.* [1993] imply. Remobilization of ^{10}Be from the sediments was deduced by *Bourlès et al.* [1989b, 1991] from the analysis of hydrothermal pore waters emanating from sediment-covered mid ocean ridges. The amount of remobilized ^{10}Be, however, was shown to be very low and negligible compared to the atmospheric supply. The influence of remobilized Be also appeared to be restricted to a small area of a few kilometers around the hydrothermal centers. These authors also demonstrated that remobilization is generally of minor importance for the use of ^{10}Be as a geochronometer in marine sediments. In the water column of the open ocean, the mean residence time varies between 400 and 1000 years [*Kusakabe et al.*, 1991; *Ku et al.*, 1990; *Segl et al.*, 1987], but it can be shorter at the ocean boundaries, where high particle fluxes account for very efficient scavenging [*Anderson et al.*, 1990].

Thorium 230 ($T_{1/2}$ = 75,200 years) and protactinium 231 ($T_{1/2}$ = 32,400 years) are produced by decay of ^{234}U and ^{235}U in the water column with a constant rate due to the homogeneous U concentration of 3.3 μg/L in the ocean, which is a result of the relatively long residence time of U in the oceans of about 400,000 years [c.f. *Mangini et al.*, 1979]. The production amounts to 2.6 disintegrations per minute (dpm)/cm^{2}kyr(1000m) water column for ^{230}Th and to 0.24 dpm/cm^{2}kyr(1000m) water column for ^{231}Pa. Both isotopes are highly particle reactive and are quickly adsorbed to particles in the water column. Important particulate adsorber phases for both isotopes are Mn and Fe oxihydroxides if their abundance is high [*Bacon and Anderson*, 1982], with Mn being more efficient in scavenging ^{231}Pa relative to ^{230}Th [*Anderson et al.*, 1983b]. The mean residence time of ^{230}Th in the oceans' water column amounts to between 20 and 40 years and the residence time of ^{231}Pa is about 100 years [*Anderson et al.*, 1983a; *Nozaki et al.*, 1981]. It is generally accepted that no remobilization of both isotopes in the sediments occurs [e.g., *Ivanovich and Harmon*, 1992]. The mother isotope U can be very mobile in the sediments under certain conditions, but as long as there are no strong variations and peaks observable in the U profiles of the sediments, diagenetic mobilization can be considered unimportant.

In combination with ^{231}Pa, ^{230}Th has been used for investigating changes in hydrothermal influence on deep-sea sediments by comparing the measured fluxes to the values expected from production and by comparing the measured ^{230}Th$_{ex}$/^{231}Pa$_{ex}$ ratios to the production ratio in the water column of 10.8 [*Shimmield and Price*, 1988]. These authors found increased fluxes of both radionuclides to the sediments of the East Pacific Rise at 20°S, and they interpreted ^{230}Th$_{ex}$/^{231}Pa$_{ex}$ activity ratios in the range of 3-4 as a consequence of hydrothermal activity. The few available water column data yield activity ratios of the two radionuclides in the range from 3 to 5, reflecting the stronger affinity of ^{230}Th to particles. Correspondingly, the ratio in deep-sea sediments from the Central Pacific is increased to values between 20 and 30 [*Yang et al.*, 1986], whereas in areas of enhanced particle fluxes the low ratio of the water column is transferred to the sediments.

We studied the influence of hydrothermal activity on the Galapagos microplate deep-sea sediments by comparing the fluxes of ^{230}Th$_{ex}$ and ^{10}Be. The enhanced hydrothermal supply of Mn and Fe oxyhydroxides should result in an increased flux of ^{230}Th to the sediments, whereas ^{10}Be should not be affected by this on the same scale. We suggest a model that was presented by *Eisenhauer et al.* [1987] to trace periods of enhanced paleoproductivity in the northwest Pacific but that can serve as a tool to trace hydrothermal activity as well. This model compares the fluxes of the two radionuclides ^{10}Be and ^{230}Th that exceed production and is described in detail in the hydrothermalism section. The model predicts a ^{10}Be/^{230}Th$_{(F/P)}$ ratio of 4, which is the square root of the ratio of the mean residence times of the two radionuclides in the water column in a center of biological activity. It also predicts an increase of this ratio to values above 4 in a certain distance from the area of the high particle fluxes. In agreement with this prediction, ratios $\geq$ 4 were observed, for example, in the upwelling area off West Africa [*Mangini et al.*, 1984] and in the Fram Strait [*Eisenhauer et al.*, 1990]. The model does not allow ratios below 4. However, as observed in high-resolution profiles of the two radionuclides of various sediment cores, peak concentrations of ^{230}Th give rise to values significantly below 4 which were called ^{230}Th anomalies [*Eisenhauer et al.*, 1987, 1990]. These anomalies were attributed to a selective scavenging process of ^{230}Th caused by enhanced deposition of Mn. In the water column overlying hydrothermally active mid ocean ridges, which are the major sources of Mn in the ocean, we expect preferential scavenging and lateral supply of ^{230}Th, that is, ^{10}Be/^{230}Th$_{(F/P)}$ ratios that can be lower than 4 in the associated sediments during periods of hydrothermal activity.

To test this prediction, we measured the depth profiles of the assumed hydrothermal ^{230}Th carrier phases, Mn and Fe in sediments close to the hydrothermal centers of the Galapagos microplate. The distribution of the Mn concentration in surface sediments of the eastern Equatorial Pacific was described by *Berger et al.* [1983]. They observed two distinct peaks of Mn in the upper 40 cm of the sediments that they ascribed to remobilization of Mn in sections of the se-

diments lower than 10 cm and to its reprecipitation at the redoxcline. According to these authors, Mn is transported by burrowing organisms from the oxidizing into the reducing environment and is then mobilized and moves upward until it reprecipitates at the redoxcline. In their model the upper peak is interpreted as being the recent redoxcline enrichment. The second, subsurface Mn spike [*Berger et al.*, 1983] is attributed to enhanced activity of benthic organisms during the last glacial period due to high food supply to the deep water. According to their model, by the end of the last glacial period, the fertility of the ocean dropped and the food supply to the deep water was diminished, and the burrowers were not as active as before. As a consequence, the manganese enrichment in the subsurface peak could only partly be mobilized upward and remained in place in the sediment. The subsurface Mn spike thus represents the transition from climatic stage 2 to stage 1. *Mangini et al.* [1990] have argued that this peak could also originate from rapid precipitation of Mn from the water column. Which one of the two models comes closer to reality is still an open question.

Scavenging effects of ^{231}Pa and ^{10}Be resulting from increased particle fluxes at the ocean boundaries have been another important field of research in the recent past [c.f. *Lao*, 1991; *Anderson et al.*, 1990; *Yang et al.*, 1986]. Increased radionuclide accumulation in the sediments of the oceans' boundaries is caused by horizontal diffusion of isotopes from areas of lower particle fluxes. Increased particle fluxes which can lead to enhanced scavenging of radionuclides mainly occur at the ocean margins. Particles originate from terrestrial sources such as fluvial input, for example, in the area of the Congo fan [*Jansen et al.*, 1987] or from aeolian input as in the Mediterranean [*Brown et al.*, 1992]. Another source of high particle fluxes are areas of high biological production induced by coastal upwelling [*Mangini and Diester-Haass*, 1983].

In this study we model the importance of hydrothermalism and paleoproductivity for the radionuclide scavenging to the sediments of the Galapagos microplate during the last 100 kyr from measurement of the radionuclides ^{230}Th, ^{231}Pa, and ^{10}Be, and the elements Mn and Fe. The sediments of the microplate were influenced by different processes causing enhanced fluxes of particles which result in enhanced fluxes of the radionuclides to the sediments: high biological productivity of the surface waters in the equatorial divergence zone of the eastern Equatorial Pacific Ocean and spatial variations of this zone as, for example, an extension during the last glacial [*Sarnthein and Winn*, 1990] caused changes in biogenic particle fluxes and thus in the scavenging of ^{10}Be and ^{231}Pa. Superimposed on this process may be the effects of varying boundary-scavenging intensity induced by enhanced paleoproductivity at the centers of coastal upwelling off Peru [*Oberhänsli et al.*, 1990]. Finally, the hydrothermal supply of Mn and Fe oxyhydroxides from the mid ocean ridges is expected to enhance the scavenging of ^{230}Th and ^{231}Pa compared to ^{10}Be.

We evaluate the influence on the fluxes of the radionuclides during the last 100 kyr applying two different models. We first discuss the boundary-scavenging model of *Anderson et al.* [1990], which assumes that ^{10}Be and ^{231}Pa are affected by lateral scavenging, whereas ^{230}Th is not. This model can only be applied as long as lateral scavenging of ^{230}Th is excluded, which probably is the case in most parts of the ocean. If there is a scavenging phase present which tends to preferably scavenge ^{230}Th, resulting in increased ^{230}Th fluxes, the boundary-scavenging model is expected to yield deposition indices that are too low. The second model of *Eisenhauer et al.* [1987] predicts the occurence of Th anomalies caused by increased supply of ^{230}Th to the sediments, related to increased supply of the carrier phases Mn and Fe [*Mangini et al.*, 1990].

Material and Methods

The two gravity cores (KLH 093: 1°29.97'N, 102°03.81' W, 3259 m water depth, 290 cm core length and KLH 068: 1°13.91'N, 101°36.73'W, 2870 m water depth, 215 cm core length) presented in this study were recovered during German research vessel *Sonne 60* cruise in January 1989 on the Galapagos microplate in the eastern Equatorial Pacific.

The Galapagos microplate is located at the triple junction of the plate boundaries between Nazca, Cocos, and the Pacific plate [*Lonsdale*, 1988]. The oldest parts of the microplate have an age of about 1 Ma.

The KLH 068 core site is located at the foot of a seamount as high as 1500 m at the SE boundary of the microplate. The site of core KLH 093 is in the southern part of the microplate at a distance of about 20 km from the active spreading centers (Figure 1).

The sediments show quite a uniform composition consisting of a foraminiferal ooze with a carbonate content between 71 and 86 % (Figure 2) and contain randomly distributed basaltic ash layers, most of which are found in core KLH 068. They do not have quantitative importance with the exception of the core section between 120 and 130 cm of core KLH 068, where the carbonate content decreases to about 35 %. These layers indicate some disturbances by volcanic activity. The color of the sediments is characterized by a brownish layer at the uppermost 50 cm followed by pale yellowish layers alternating with brownish ones. No other significant lithological or sedimentological changes were observed in both cores. For further information see the work by *Eckhardt* [1992].

The cores were sampled continously and then split with a resolution of 5 cm per sample with the exception of the upper 40 cm of core KLH 093, which was sampled with a resolution of 2 cm per sample. The measurement for each sample thus represents the average value for the corresponding 5- or 2-cm section.

Chemical Preparation

The sample material was dried and homogenized. For the measurement of ^{230}Th, ^{231}Pa, ^{238}U, and ^{234}U by α spectroscopy, 0.5-g sample material was weighed and a ^{228}Th/^{232}U spike in radioactive equilibrium with an activity of 11.2

dpm/ mL was added. The samples were dissolved in HF (30 %) and evaporated to dryness twice. After melting the residues with $LiBO_2$, they were dissolved in 8 N HCl and loaded onto a Dowex 1 X 8 ion exchange column to separate U/Fe from Th/Ca. The solution co ntaining Th was evaporated to dryness again and then dissolved in 8 N HNO_3 and loaded onto a Dowex 1 X 8 ion exchange column to separate Ca. Th was then back-extracted from the column with 8 N and 10 N HCl and evaporated to dryness again. After being e vaporated to dryness and dissolved in 8 N HNO_3, the solution containing U was loaded onto a ion exchange column to separate Fe. After back-extraction of the U with

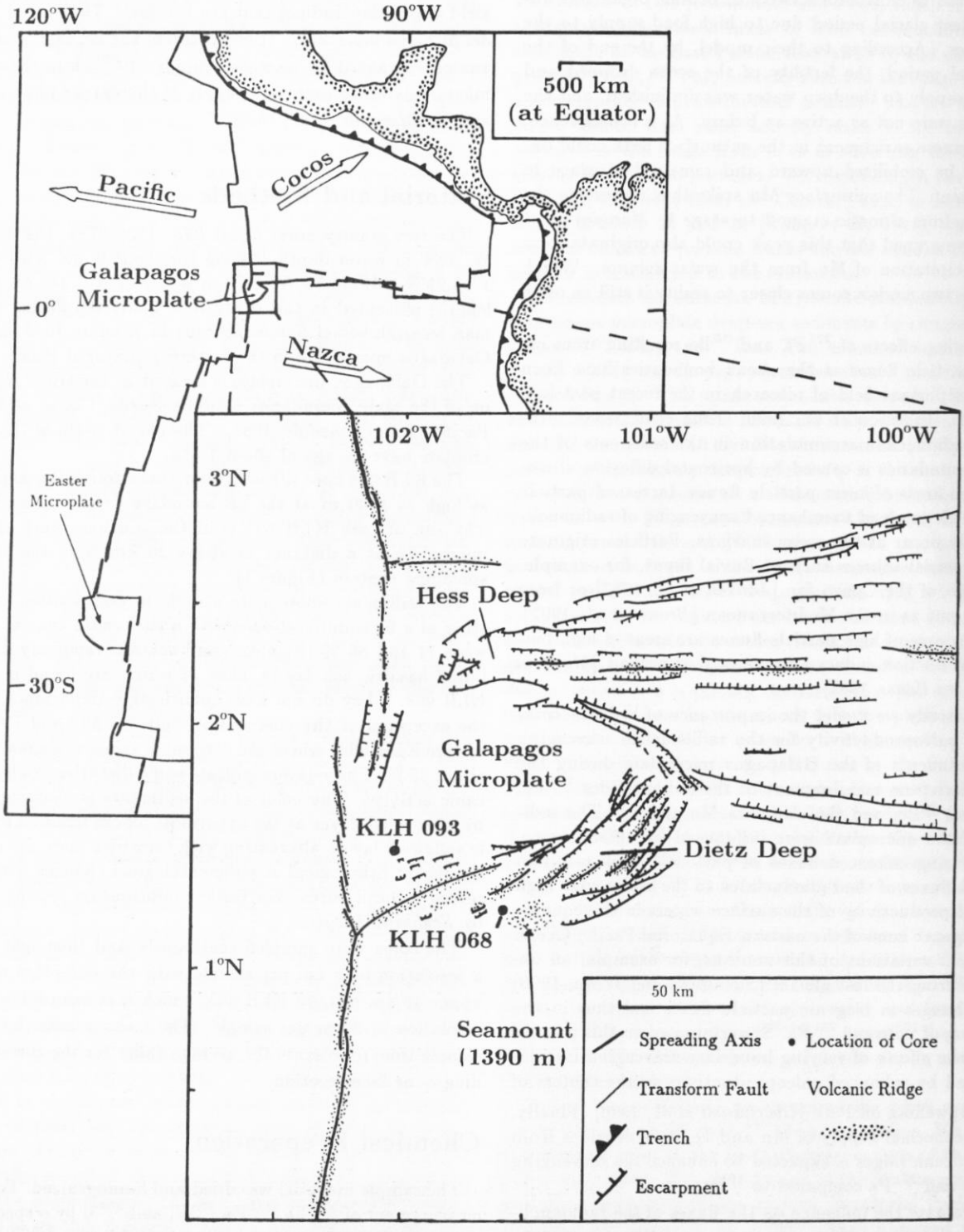

Figure 1. Map showing the coarse structural patterns of the Galapagos microplate and locations of the investigated cores. Modified after *Lonsdale* [1988].

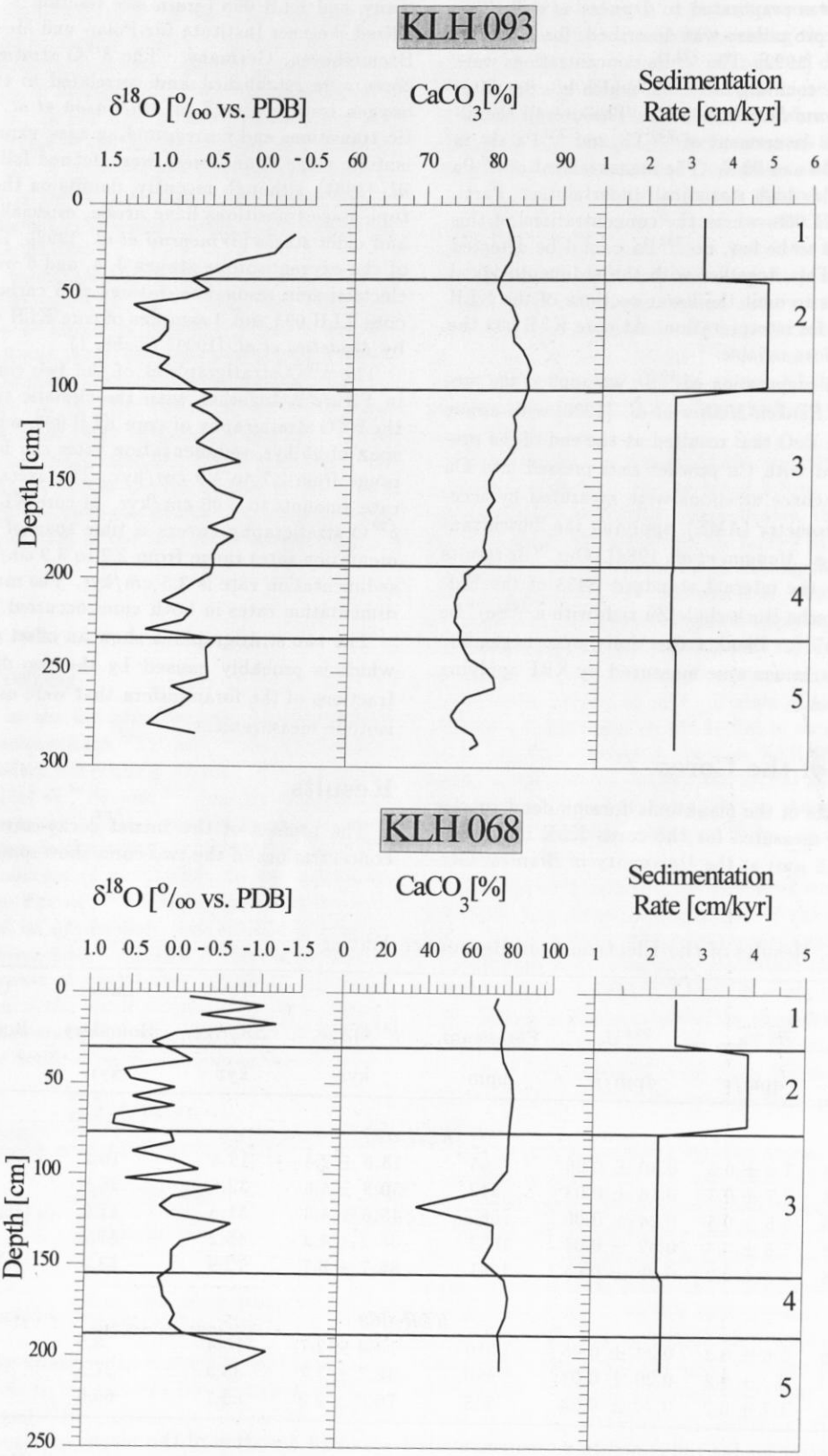

Figure 2. The $\delta^{18}O$ profiles of *N. dutertrei* of the core KLH 093 (grain size fraction > 315 μm) and of core KLH 068 (grain size fraction > 100 μm) in per mil relative to Pee Dee belemnite (PDB) versus depth in the core. The standard deviation for the measurements amounted to $\pm$ 0.07 °/oo. Additionally, the profiles of $CaCO_3$ in weight percent and the sedimentation rates in centimeters per 1000 years are plotted versus depth. The transitions of the isotope stages following *Martinson et al.* [1987] are marked by horizontal lines.

H_2O, the solution was evaporated to dryness as well. The final electroplating pro cedure was described, for example, by *Eisenhauer et al.* [1992]. The ^{231}Pa concentrations were determined by an α counting of ^{227}Th, which is a daughter of ^{231}Pa [*Mangini and Sonntag*, 1977]. The overall chemical yields for the m easurement of ^{230}Th and ^{231}Pa are in the range between 50 and 90 %. The measurement of ^{231}Pa by this method yields high statistical uncertainties. Particularly at core KLH 068, where the concentrations of this radionuclide tended to be low, no ^{231}Pa coul d be detected in many samples. This, together with the sedimentological observations, led us to omit the lower sections of the KLH 068 $^{231}Pa_{ex}$ profile for interpretation. At core KLH 093 the ^{231}Pa results are more reliable.

For the chemical preparation of ^{10}Be we applied the method described by *Henken-Mellies et al.* [1990] with minor modifications. The BeO that resulted at the end of the preparation was mixed with Cu powder and pressed into Cu targets. The ^{10}Be conce ntrations were measured by accelerator mass spectrometry (AMS), applying the Zürich tandem accelerator [e.g., *Mangini et al.*, 1984]. Our ^{10}Be results were calibrated to the internal standard S433 of the Eidgenössische Technische Hochschule Zü rich with a $^{10}Be/^{9}Be$ ratio of $101.4 \cdot 10^{-12}$. Blank corrections were negligible. Mn and Fe concentrations were measured by XRF applying standard techniques.

Chronology of the Cores

The δ^{18}O records of the planktonic foraminiferal species *N. dutertrei* were measured for the cores KLH 093 (grain size fraction > 315 μm) at the University of Bremen, Germany, and KLH 068 (grain size fraction > 100 μm) at the Alfred Wegener Institute für Polar- und Meeresforschung at Bremerhaven, Germany. The δ^{18}O stratigraphies for the cores were established and correlated to the standardized oxygen isotope record of *Martinson et al.* [1987]. Climatic transitions and corresponding ages, expressed as oxygen isotope stage boundaries, were defined following *Imbrie et al.* [1984], although recently, doubts on the age of the isotope stage transitions have arisen, especially termination II and older stages [*Winograd et al.*, 1992]. The depth in core of the oxygen isotope stages 3, 4, and 5 were confirmed by electron spin resonance datings of 5 carbonate samples of core KLH 093 and 3 samples of core KLH 068, as described by *Mudelsee et al.* [1991] (Table 1).

The δ^{18}O stratigraphies of the two cores are displayed in Figure 2, together with the climatic transitions. From the δ^{18}O stratigraphy of core KLH 093, which covers a time span of 95 kyr, sedimentation rates can be calculated that range from 2.7 to 4.9 cm/kyr. The average sedimentation rate amounts to 3.05 cm/kyr. In core KLH 068, where the δ^{18}O stratigraphy covers a time span of 85 kyr, the sedimentation rates range from 2.2 to 3.9 cm/kyr. The average sedimentation rate is 2.5 cm/kyr. The maximum of the sedimentation rates in both cores occurred in glacial stage 2.

The two stratigraphies show an offset of about 0.7 °/₀₀, which is probably caused by the two different grain size fractions of the foraminifera that were used for the oxygen isotope measurement.

Results

The profiles of the initial decay-corrected radionuclide concentrations of the two cores show some striking features,

Table 1. Results of the Electron Spin Resonance Dating

Depth, cm	$^{230}Th_{ex}$, dpm/g	^{234}U, dpm/g	Potassium, ppm	δ^{18}OAge, kyr	ESR Age, kyr	Lower Boundary, kyr	Upper Boundary, kyr
			KLH 093				
55- 58	7.4 ± 0.3	0.30 ± 0.06	565	13.6 ± 2.4	13.4	10.2	16.8
115-118	3.7 ± 0.3	0.18 ± 0.03	542	30.8 ± 6.6	32.6	26.9	39.0
155-158	5.6 ± 0.3	0.24 ± 0.06	665	45.6 ± 4.3	51.8	41.6	64.4
215-218	7.6 ± 0.3	0.32 ± 0.05	1082	68.2 ± 4.3	45.2	37.2	54.3
265-268	7.3 ± 0.2	0.29 ± 0.04	1061	86.7 ± 6.7	72.9	53.3	100.9
			KLH 068				
40- 50	5.6 ± 0.2	0.34 ± 0.05	510	13.0 ± 2.7	16.4	8.9	24.6
100-110	3.2 ± 0.2	0.20 ± 0.04	490	36.7 ± 7.7	35.3	27.5	44.3
190-200	1.7 ± 0.2	0.24 ± 0.03	503	76.6 ± 2.2	85.7	69.0	106.3

The error for the radionuclide measurements is 1 standard deviation of the mean.

The δ^{18}O ages of the sampled intervals were determined by correlation to the stacked δ^{18}O record of *Martinson et al.* [1987].

The last three columns show the results of the electron spin resonance (ESR) dating in kiloyears and the error intervals toward lower and higher ages.

Note that dpm indicates disintegrations per minute, and ppm indicates parts per million.

which are presented in Figure 3. In the KLH 093 core sections corresponding to isotope stages 1, 2, and 3, no significant variations of the radionuclide concentrations occurred, with the exception of increased $^{231}Pa_{ex}$ concentrations in the stage 1 section. In the core sections representing stages 4 and 5 an increase of the concentrations by a factor of about 2 is observed. A synchronous increase of 1 order of magnitude occurs in the Mn/Fe ratio. The higher Mn/Fe ratio in the core section representing stage 1 is not reflected in the radionuclide profiles.

No such strong variations can be found in the profiles of core KLH 068. The values of the $^{230}Th_{ex}$ and ^{10}Be concentrations tend to be higher in stages 1, 2, and 4, but the variations are small and partly coincide with layers of basaltic ash, which dilute the concentrations as, for example, at a core depth of about 120 cm. The values of the $^{230}Th_{ex}$ concentrations, and in most parts of the core also the $^{231}Pa_{ex}$ concentrations, do not reach the ones of core KLH 093. The variations of the Mn/Fe profile are not as distinct as in core KLH 093, although the two core profiles do resemble each other. In Table 2 all data of the two cores are provided.

Discussion

Boundary Scavenging

As pointed out in the introduction, the concentrations and fluxes of the radionuclides ^{10}Be and ^{231}Pa are strongly influenced by boundary scavenging effects. We calculated deposition indices (I_d) of ^{10}Be and $^{231}Pa_{ex}$ by normalizing their concentrations to the $^{230}Th_{ex}$ concentrations and then compared these ratios to the ratios expected from production as done by *Anderson et al.* [1990]. In this approach the regional average flux of ^{230}Th from the water column is assumed to equal its production, and no lateral supply is allowed. The radionuclides ^{10}Be and ^{231}Pa can be transported laterally because of their lower reactivity and thus higher residence time in the water column. For the I_d calculation we applied the expected production of ^{230}Th for the corresponding water depth of each core (equations (1)-(3)).

$$I_d(Pa) = \frac{\frac{^{231}Pa_{ex}}{^{230}Th_{ex}}\text{dec.corr.}}{\frac{^{231}Pa}{^{230}Th}\text{ production ratio (0.093)}} \quad (1)$$

$$I_d(Be) = \frac{\frac{^{10}Be}{^{230}Th_{ex}}\text{dec.corr.}}{\frac{^{10}Be}{^{230}Th}\text{expected}} \quad (2)$$

with

$$\frac{^{10}Be}{^{230}Th}\text{expected} = \frac{\text{glob.}\,^{10}Be\text{ production}}{^{230}Th\text{ production}} \quad (3)$$

$I_d = 1$ means that the measured radionuclide concentration is equal to production, $I_d > 1$ stands for an import of the radionuclides ^{231}Pa and ^{10}Be relative to ^{230}Th from other areas, and $I_d < 1$ means an export of the radionuclides to other areas.

The calculations of the two cores show that the I_d values are higher than 1 during the last 100 kyr except the $I_d(Pa)$ in the sections between 10 and 40 kyr and the $I_d(Be)$ in the section at around 18 kyr in core KLH 093 where there are values slightly below 1. For both cores the $I_d(Be)$ profiles were additionally calculated assuming the same production rate variations as given by *Mazaud et al.* [1991] for ^{14}C (Figure 4). I_d values greater than 1 are exactly what we would expect, because the sediments were located under the equatorial high-bioproductivity zone of the surface waters throughout the last 30 kyr [*Sarnthein and Winn*, 1990] and probably also throughout the last 100 kyr, so that enhanced scavenging of ^{10}Be and ^{231}Pa occurred. Our I_d values for the surface sediments agree quite well with the measurements of *Anderson et al.* [1990] and *Lao* [1991], who gave I_d values around 2 for sediments located northwest and northeast of the Galapagos microplate. We determined surface I_d values of 1.59 for ^{10}Be and 1.82 for ^{231}Pa at core KLH 093 and 2.56 and 0.98 for ^{10}Be and $^{231}Pa_{ex}$ at core KLH 068, respectively, presumably because of a stronger hydrothermal influence at the KLH 093 site.

The I_d values in cores KLH 093 and 068 show significant downcore variations, but as noted before, the ^{231}Pa results are much more uncertain. Nevertheless, they remain valuable to confirm the trends of the $I_d(Be)$ profiles. $I_d(Be)$ values which were calculated as accounting for production rate changes similar to ^{14}C [*Mazaud et al.*, 1991] are significantly lower than the ones calculated applying the present-day production rate in the core sections representing the isotope stages 2-4, and relative variations of the $I_d(Be)$ profile appear more clearly in part. Minima of the $I_d(Be)$ in both cores and a minimum of the $I_d(Pa)$ in core KLH 093 occur in the middle of stage 2. In core KLH 093 there are also minor minima of the $I_d(Be)$ and $I_d(Pa)$ at the beginning of isotope stage 4 and of the $I_d(Be)$ in the middle of stage 3 where, unfortunately, only one $^{231}Pa_{ex}$ concentration could be measured.

To explain the minima, we compared our I_d record to the upwelling history and the intensity of paleoproductivity off South America deduced from grain size analyses and benthic foraminiferal assemblages in sediments underlying the upwelling centers off Peru [*Oberhänsli et al.*, 1990]. Oberhänsli et al. determined 3 maxima of the intensity of paleoproductivity for the last 100 kyr. One major maximum occurred in the second half of glacial stage 2 and two minor ones around 45 kyr and 72 kyr B.P. We marked these periods of time in Figure 4.

These paleoproductivity maxima appear to coincide with I_d minima in our cores. In core KLH 093 the I_d profiles of both radionuclides show relative minima in the core sections temporally corresponding to the paleoproductivity maxima off Peru. The only exception is the 40- to 45-kyr minimum in the $I_d(Pa)$ profile, where the $^{231}Pa_{ex}$ concentrations were mostly too low for a reliable measurement. For the reasons mentioned above, in core KLH 068 this coincidence apparently only occurs for the $I_d(Be)$ at the maximum at the end of stage 2 and for the production rate corrected $I_d(Be)$ record at the 40- to 45-kyr maximum. In general, the ^{231}Pa does not seem to be influenced by these effects as strongly as the ^{10}Be.

A strong decrease of the deposition of ^{10}Be in the core section representing the period around 18 kyr B.P. occurs, although *Lao et al.* [1992a] deduced a 30 % production increase of this radionuclide during the last glacial maximum.

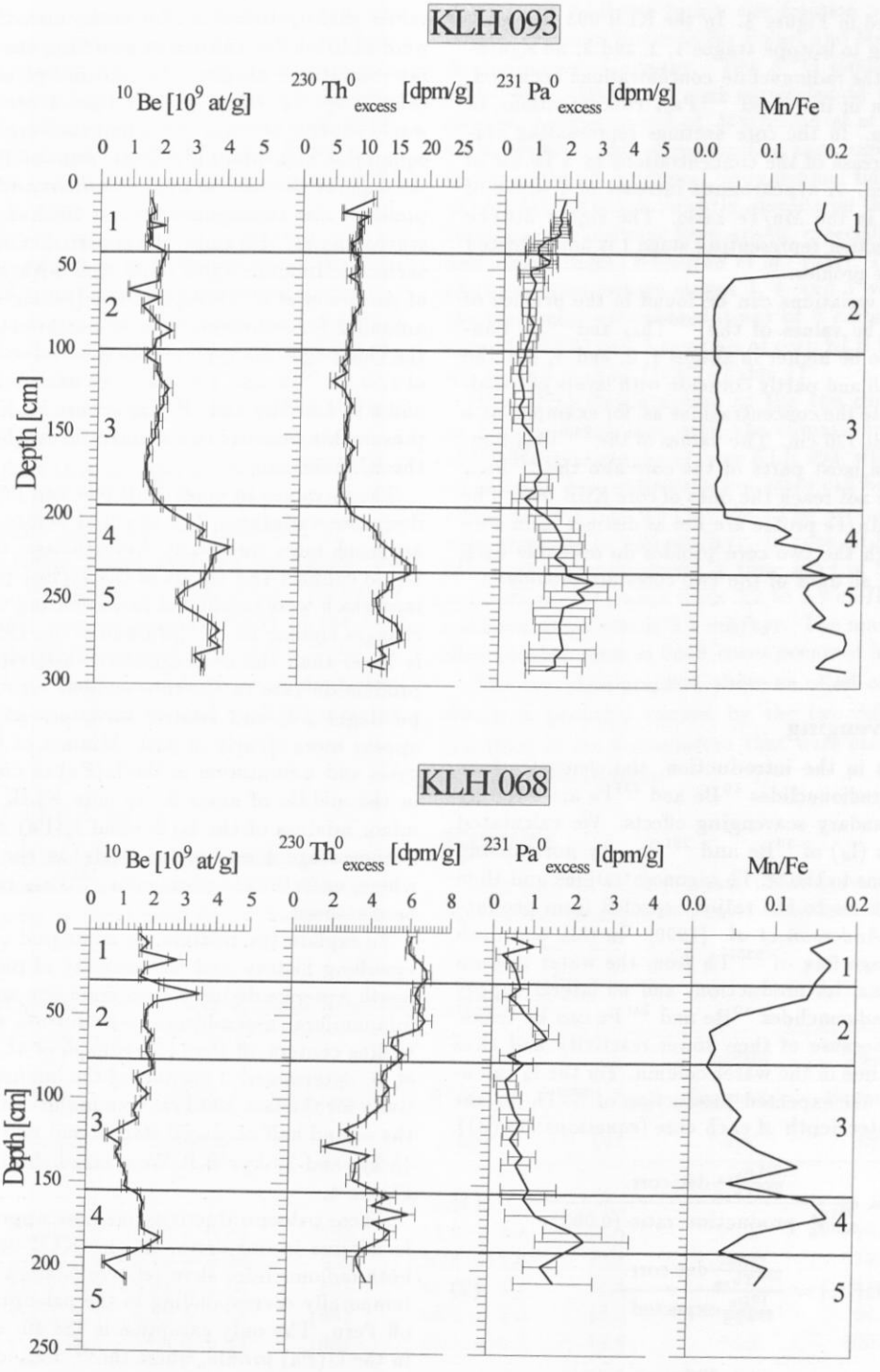

Figure 3. Measured profiles of ^{10}Be in 10^9 atoms per gram, of the Mn/Fe ratios, and of the decay-corrected profiles of $^{230}Th^0_{ex}$ and $^{231}Pa^0_{ex}$ in disintegrations per minute per gram versus depth in core. The $^{231}Pa^0_{ex}$ concentrations of core KLH 093 represent three-point running means of the decay corrected concentrations. The transitions of the isotope stages are marked by horizontal lines. The errors are 1 standard deviation of the mean and do not comprise age uncertainties of the dating, which are negligible compared to the measurement statistics. Note the different scales of the $^{230}Th^0_{ex}$ concentrations of the two cores.

Table 2. Results of Core KLH 093

Depth, cm	Age, ky	DBD, g/cm^3	$^{231}Pa_{ex}$, dpm/g	^{234}U, dpm/g	$^{230}Th_{ex}$, dpm/g	^{10}Be ($\cdot 10^9$ at/g)	Depth, cm	$\delta^{18}O$, ‰	MnO, wt %	Fe_2O_3, wt %	$CaCO_3$, wt %
					KLH 093						
7.5	2.3	0.58	1.78 ± 0.31	0.27 ± 0.06	11.03 ± 0.28	1.60 ± 0.04	7.5	n.d.	0.29	1.61	81.5
16.0	4.8	0.59	n.d. ± n.d.	0.22 ± 0.06	5.81 ± 0.13	1.73 ± 0.04	15	-0.303	0.27	1.53	82.3
18.0	5.4	0.61	1.19 ± 0.18	0.29 ± 0.05	9.91 ± 0.21	1.56 ± 0.05					
20.0	6.0	0.63	1.83 ± 0.19	0.22 ± 0.06	8.81 ± 0.21	1.57 ± 0.05	20	-0.193	0.28	1.68	82.6
22.0	6.6	0.64	1.60 ± 0.27	0.28 ± 0.06	8.10 ± 0.25	1.57 ± 0.04					
24.0	7.2	0.65	1.16 ± 0.21	0.31 ± 0.08	8.75 ± 0.22	2.06 ± 0.05	25	-0.091	0.32	1.89	82.7
26.0	7.8	0.65	1.56 ± 0.21	0.27 ± 0.04	8.32 ± 0.21	1.50 ± 0.04					
28.0	8.4	0.64	1.61 ± 0.28	0.25 ± 0.04	8.14 ± 0.30	1.60 ± 0.05					
30.0	9.0	0.63	1.17 ± 0.30	0.19 ± 0.03	8.23 ± 0.26	1.59 ± 0.04	30	0.270	0.38	2.07	82.2
32.0	9.6	0.62	1.18 ± 0.41	0.23 ± 0.06	7.83 ± 0.34	1.61 ± 0.05					
34.0	10.2	0.62	0.74 ± 0.18	0.28 ± 0.04	6.74 ± 0.23	1.46 ± 0.04	35	0.484	0.49	2.23	81.4
36.0	10.8	0.62	0.92 ± 0.35	0.23 ± 0.06	7.10 ± 0.32	n.d. ± n.d.					
38.0	11.4	0.62	0.81 ± 0.20	0.22 ± 0.04	6.81 ± 0.20	n.d. ± n.d.					
40.0	12.0	0.62	0.79 ± 0.40	0.28 ± 0.06	6.87 ± 0.31	2.09 ± 0.06	40	0.698	0.56	2.49	80.6
42.0	12.4	0.60	n.d. ± n.d.	0.24 ± 0.06	7.89 ± 0.21	n.d. ± n.d.					
44.0	12.8	0.58	0.98 ± 0.16	0.23 ± 0.04	7.55 ± 0.16	1.99 ± 0.05	45	0.533	0.45	2.40	80.3
46.0	13.2	0.58	1.13 ± 0.17	0.31 ± 0.05	7.57 ± 0.20	n.d. ± n.d.					
48.0	13.6	0.58	1.00 ± 0.30	0.28 ± 0.04	7.72 ± 0.23	n.d. ± n.d.					
50.0	14.0	0.58	0.44 ± 0.30	0.30 ± 0.05	7.86 ± 0.36	1.91 ± 0.05	50	0.743	0.33	2.21	81.1
52.0	14.4	0.60	0.41 ± 0.23	0.24 ± 0.06	7.36 ± 0.26	n.d. ± n.d.					
54.0	14.9	0.62	0.93 ± 0.34	0.22 ± 0.06	6.20 ± 0.31	1.85 ± 0.06	55	1.213	0.09	1.99	82.5
57.5	15.6	0.62	0.55 ± 0.28	0.30 ± 0.06	7.42 ± 0.31	1.86 ± 0.07					
62.5	16.6	0.59	0.62 ± 0.20	0.20 ± 0.04	7.61 ± 0.23	0.88 ± 0.02	65	0.908	0.04	1.42	83.4
67.5	17.6	0.60	0.72 ± 0.17	0.29 ± 0.08	7.81 ± 0.29	1.92 ± 0.05	70	0.910	0.03	1.44	82.7
72.5	18.6	0.61	0.27 ± 0.10	0.13 ± 0.02	7.58 ± 0.18	1.35 ± 0.04	75	0.974	0.02	1.15	82.9
77.5	19.7	0.62	0.60 ± 0.17	0.20 ± 0.03	6.64 ± 0.21	1.65 ± 0.05	80	1.124	0.02	1.17	84.2
82.5	20.7	0.62	0.67 ± 0.12	0.22 ± 0.04	6.67 ± 0.22	1.84 ± 0.05	85	0.889	0.02	1.13	84.9
87.5	21.7	0.65	0.55 ± 0.11	0.17 ± 0.04	5.99 ± 0.20	2.29 ± 0.07	90	0.969	0.02	1.04	85.5
92.5	22.7	0.62	0.39 ± 0.19	0.11 ± 0.03	6.10 ± 0.22	1.82 ± 0.12	95	0.811	0.02	1.09	85.0
97.5	23.7	0.62	0.51 ± 0.15	0.15 ± 0.06	5.71 ± 0.23	1.75 ± 0.05	100	0.674	0.02	1.07	85.2
102.5	25.3	0.63	0.34 ± 0.08	0.19 ± 0.02	5.75 ± 0.12	1.48 ± 0.05	105	0.480	0.02	1.06	84.8
107.5	27.1	0.62	0.33 ± 0.16	0.13 ± 0.03	4.81 ± 0.20	1.87 ± 0.06	110	0.671	0.03	1.15	84.3
112.5	29.0	0.58	0.22 ± 0.12	0.27 ± 0.05	5.39 ± 0.21	1.85 ± 0.10	115	0.488	0.03	1.34	83.1
117.5	30.8	0.59	n.d. ± n.d.	0.18 ± 0.03	3.67 ± 0.30	1.98 ± 0.04	120	0.376	0.03	1.40	83.4
122.5	32.7	0.60	0.43 ± 0.12	0.15 ± 0.04	4.90 ± 0.16	2.22 ± 0.13	125	0.509	0.03	1.38	83.3

Table 2. (continued)

Depth, cm	Age, ky	DBD, g/cm^3	$^{231}Pa_{ex}$, dpm/g	^{234}U, dpm/g	$^{230}Th_{ex}$, dpm/g	^{10}Be ($\cdot 10^9$ at/g)	Depth, cm	$\delta^{18}O$, ‰	MnO, wt %	Fe_2O_3, wt %	$CaCO_3$, wt %
127.5	34.5	0.57	0.20 ± 0.17	0.17 ± 0.05	5.23 ± 0.25	2.05 ± 0.12	130	0.618	0.03	1.22	83.4
132.5	36.4	0.60	0.32 ± 0.11	0.19 ± 0.05	5.76 ± 0.22	2.07 ± 0.12	135	0.420	0.03	1.28	82.6
137.5	38.2	0.57	0.21 ± 0.11	0.17 ± 0.03	5.15 ± 0.15	1.89 ± 0.05	140	0.197	0.04	1.40	81.6
142.5	40.1	0.57	0.33 ± 0.17	0.15 ± 0.09	4.84 ± 0.22	1.92 ± 0.12	145	0.590	0.04	1.52	80.2
147.5	41.9	0.53	n.d. ± n.d.	0.24 ± 0.06	4.88 ± 0.21	1.80 ± 0.11	150	0.519	0.04	1.67	79.5
152.5	43.7	0.56	0.51 ± 0.12	0.20 ± 0.04	4.65 ± 0.17	1.83 ± 0.11	155	0.411	0.04	1.66	79.6
157.5	45.6	0.54	n.d. ± n.d.	0.24 ± 0.06	5.56 ± 0.31	1.59 ± 0.04	160	0.164	0.04	1.57	80.4
162.5	47.4	0.55	n.d. ± n.d.	0.24 ± 0.05	4.76 ± 0.21	1.65 ± 0.10	165	0.218	0.04	1.60	79.4
167.5	49.3	0.53	n.d. ± n.d.	0.24 ± 0.06	4.78 ± 0.21	1.54 ± 0.04	170	0.260	0.05	1.63	79.9
172.5	51.1	0.51	0.27 ± 0.13	0.24 ± 0.06	4.26 ± 0.17	1.55 ± 0.04	175	0.486	0.05	1.69	79.3
177.5	53.0	0.51	0.54 ± 0.21	0.24 ± 0.04	4.02 ± 0.22	1.55 ± 0.09	180	0.243	0.04	1.75	79.2
182.5	54.8	0.51	0.19 ± 0.09	0.23 ± 0.04	3.77 ± 0.15	1.71 ± 0.04	185	0.390	0.04	1.67	78.9
187.5	56.7	0.52	0.28 ± 0.18	0.26 ± 0.05	3.89 ± 0.22	1.84 ± 0.04	190	0.436	0.05	1.72	79.3
192.5	58.5	0.49	0.18 ± 0.09	0.23 ± 0.03	4.37 ± 0.20	2.06 ± 0.04	195	0.429	0.07	1.93	78.0
197.5	60.7	0.47	0.38 ± 0.11	0.27 ± 0.04	4.72 ± 0.17	2.44 ± 0.04	200	0.456	0.08	2.19	76.3
202.5	62.6	0.48	0.55 ± 0.20	0.25 ± 0.04	6.00 ± 0.25	2.93 ± 0.05	205	0.608	0.20	1.76	76.4
207.5	64.4	0.46	0.38 ± 0.15	0.18 ± 0.04	6.72 ± 0.22	3.44 ± 0.06	210	0.737	0.27	1.98	75.3
212.5	66.3	0.46	0.45 ± 0.13	0.34 ± 0.05	6.83 ± 0.21	3.22 ± 0.06	215	0.890	0.29	2.59	75.0
217.5	68.2	0.47	0.57 ± 0.21	0.32 ± 0.05	7.56 ± 0.30	4.23 ± 0.07	220	0.630	0.53	2.87	75.2
222.5	70.0	0.49	0.32 ± 0.10	0.29 ± 0.05	8.26 ± 0.30	3.72 ± 0.07	225	0.708	0.47	2.66	75.0
227.5	71.9	0.53	0.27 ± 0.09	0.31 ± 0.06	9.11 ± 0.31	3.67 ± 0.05	230	1.034	0.43	2.79	75.9
232.5	73.8	0.53	0.73 ± 0.15	0.27 ± 0.08	8.95 ± 0.47	3.54 ± 0.07	235	0.392	0.49	2.47	75.8
237.5	76.0	0.54	0.28 ± 0.16	0.24 ± 0.04	7.21 ± 0.22	3.39 ± 0.05	240	0.481	0.40	2.43	76.4
242.5	77.8	0.53	0.72 ± 0.25	0.27 ± 0.04	6.90 ± 0.36	2.87 ± 0.05	245	n.d.	0.39	2.48	77.2
247.5	79.6	0.54	0.36 ± 0.16	0.20 ± 0.05	5.91 ± 0.25	2.59 ± 0.04	250	0.469	0.38	2.28	79.5
252.5	81.3	0.55	0.37 ± 0.16	0.20 ± 0.09	5.90 ± 0.25	2.72 ± 0.05	255	0.461	0.38	2.14	80.7
257.5	83.1	0.57	0.32 ± 0.18	0.39 ± 0.04	6.10 ± 0.23	3.17 ± 0.09	260	0.794	0.39	2.06	80.9
262.5	84.9	0.53	0.30 ± 0.11	0.34 ± 0.04	7.01 ± 0.18	3.64 ± 0.05	265	0.604	0.43	2.52	76.9
267.5	86.7	0.53	0.30 ± 0.09	0.29 ± 0.04	7.26 ± 0.16	3.94 ± 0.12	270	0.713	0.58	2.65	75.6
272.5	88.5	0.54	n.d. ± n.d.	0.22 ± 0.05	7.30 ± 0.22	3.63 ± 0.05	275	0.891	0.60	2.69	74.8
277.5	90.3	0.55	0.24 ± 0.14	0.27 ± 0.04	5.62 ± 0.20	3.97 ± 0.09	280	0.999	0.55	2.52	75.6
282.5	92.1	0.55	0.33 ± 0.16	0.24 ± 0.06	6.03 ± 0.21	3.15 ± 0.05	285	0.565	0.45	2.36	77.9
287.5	93.9	0.54	0.17 ± 0.09	0.24 ± 0.06	4.68 ± 0.30	3.45 ± 0.05	287.5	n.d.	0.42	2.37	78.6
290.0	94.8	0.53	0.23 ± 0.08	0.36 ± 0.07	5.79 ± 0.17	3.42 ± 0.05	290	n.d.	0.54	2.42	77.5

Table 2. (continued)

Depth, cm	Age, ky	DBD, g/cm^3	$^{231}Pa_{ex}$, dpm/g	^{234}U, dpm/g	$^{230}Th_{ex}$, dpm/g	^{10}Be ($\cdot 10^9$ at/g)	Depth, cm	$\delta^{18}O$, ‰	MnO, wt %	Fe_2O_3, wt %	$CaCO_3$, wt %
					KLH 068						
2.5	1.0	0.56	0.43 ± 0.15	0.24 ± 0.06	6.02 ± 0.23	1.58 ± 0.05	0	-0.154	0.26	1.56	73.3
7.5	3.0	0.60	0.93 ± 0.17	0.30 ± 0.06	5.76 ± 0.13	1.88 ± 0.08	10	-1.033	0.24	1.71	71.5
12.5	5.0	0.62	0.19 ± 0.16	0.31 ± 0.09	5.68 ± 0.20	1.61 ± 0.05	15	-0.289			
17.5	7.0	0.63	0.39 ± 0.13	0.30 ± 0.05	6.03 ± 0.19	2.78 ± 0.30	20	-1.188	0.27	1.64	76.4
22.5	9.0	0.62	0.46 ± 0.15	0.26 ± 0.06	6.28 ± 0.20	1.79 ± 0.05					
27.5	11.0	0.60	n.d. ± n.d.	0.30 ± 0.05	6.18 ± 0.21	1.60 ± 0.04	30	0.246	0.3	2.04	75.1
32.5	12.6	0.59	0.51 ± 0.16	0.30 ± 0.06	5.72 ± 0.25	2.29 ± 0.08					
37.5	13.9	0.58	0.29 ± 0.13	0.34 ± 0.04	5.51 ± 0.19	3.50 ± 0.09	40	-0.193	0.28	2.05	76.4
42.5	15.2	0.60	0.47 ± 0.17	0.37 ± 0.04	5.66 ± 0.20	2.10 ± 0.07	45	0.559			
47.5	16.5	0.62	0.55 ± 0.23	0.31 ± 0.05	5.52 ± 0.21	1.82 ± 0.07	50	0.488	0.09	1.64	80.9
52.5	17.8	0.63	n.d. ± n.d.	0.26 ± 0.06	5.76 ± 0.31	1.80 ± 0.05					
57.5	19.0	0.63	0.80 ± 0.14	0.21 ± 0.03	5.39 ± 0.18	1.78 ± 0.11	60	0.462	0.02	0.9	81.4
62.5	20.3	0.63	0.88 ± 0.20	0.30 ± 0.07	4.30 ± 0.19	2.04 ± 0.05					
67.5	21.6	0.62	n.d. ± n.d.	0.32 ± 0.05	4.18 ± 0.30	1.88 ± 0.05	70	0.668	0.03	1.04	80.5
72.5	22.9	0.63	0.24 ± 0.14	0.26 ± 0.06	4.62 ± 0.21	1.86 ± 0.16	75	0.685			
77.5	24.2	0.64	0.46 ± 0.16	0.26 ± 0.05	4.29 ± 0.21	2.02 ± 0.07	80	0.033	0.03	1.53	79.7
82.5	26.5	0.67	n.d. ± n.d.	0.25 ± 0.05	3.74 ± 0.12	2.07 ± 0.06					
87.5	28.8	0.69	0.18 ± 0.17	0.31 ± 0.09	3.57 ± 0.18	1.51 ± 0.07	90	0.453	0.06	1.74	79.4
92.5	31.0	0.68	0.20 ± 0.18	0.42 ± 0.11	3.79 ± 0.20	1.64 ± 0.05					
97.5	33.3	0.67	0.22 ± 0.18	0.31 ± 0.06	3.47 ± 0.24	1.94 ± 0.06	100	-0.294	0.04	0.98	79.0
102.5	35.6	0.68	n.d. ± n.d.	0.25 ± 0.04	3.39 ± 0.16	1.62 ± 0.09	105	0.529			
107.5	37.9	0.69	0.26 ± 0.18	0.14 ± 0.05	2.96 ± 0.18	1.45 ± 0.04	110	-0.576	0.09	1.52	71.6
112.5	40.1	0.75	0.31 ± 0.15	0.24 ± 0.06	2.55 ± 0.15	1.59 ± 0.04					
117.5	42.4	0.80	0.25 ± 0.14	0.23 ± 0.04	1.84 ± 0.16	1.07 ± 0.07	120	0.137	0.24	5.26	35.5
122.5	44.7	0.77	0.18 ± 0.08	0.22 ± 0.02	2.19 ± 0.08	0.60 ± 0.04					
127.5	47.0	0.74	n.d. ± n.d.	0.19 ± 0.03	1.12 ± 0.07	1.04 ± 0.04	130	-0.648	0.13	1.65	72.2
132.5	49.2	0.61	0.27 ± 0.13	0.16 ± 0.03	2.62 ± 0.14	0.90 ± 0.02	135	-0.463			
137.5	51.5	0.67	0.20 ± 0.13	0.24 ± 0.06	2.08 ± 0.13	1.02 ± 0.04	140	-0.101	0.14	1.09	72.0
142.5	53.8	0.67	n.d. ± n.d.	0.23 ± 0.04	2.03 ± 0.14	1.18 ± 0.03					
147.5	56.0	0.66	n.d. ± n.d.	0.32 ± 0.13	1.92 ± 0.20	1.26 ± 0.03	150		0.05	1.13	67.4
152.5	58.3	0.69	0.27 ± 0.20	0.14 ± 0.04	2.48 ± 0.17	1.19 ± 0.09					
157.5	60.1	0.72	0.23 ± 0.17	0.25 ± 0.13	2.94 ± 0.20	1.70 ± 0.06	160	0.136	0.17	1.17	78.1
162.5	62.3	0.73	n.d. ± n.d.	0.22 ± 0.04	2.39 ± 0.14	1.83 ± 0.05	165	0.098			
167.5	64.4	0.74	0.29 ± 0.19	0.19 ± 0.03	3.37 ± 0.19	1.76 ± 0.05	170	0.081	0.18	1.1	80.2
172.5	66.6	0.73	n.d. ± n.d.	0.22 ± 0.04	2.30 ± 0.22	1.78 ± 0.06					

Table 2. (continued)

Depth, cm	Age, ky	DBD, g/cm^3	$^{231}Pa_{ex}$, dpm/g	^{234}U, dpm/g	$^{230}Th_{ex}$, dpm/g	^{10}Be ($\cdot 10^9$ at/g)	Depth, cm	$\delta^{18}O$, ‰	MnO, wt %	Fe_2O_3, wt %	$CaCO_3$, wt %
177.5	68.8	0.72	0.48 ± 0.17	0.18 ± 0.04	2.76 ± 0.16	1.81 ± 0.08	180	-0.047	0.08	1.15	79.1
182.5	70.0	0.69	0.51 ± 0.27	0.24 ± 0.06	2.50 ± 0.20	2.39 ± 0.06					
187.5	73.1	0.66	n.d. ± n.d.	0.45 ± 0.04	1.95 ± 0.10	1.98 ± 0.13	190	-0.141	0.04	1.07	75.4
192.5	75.5	0.67	n.d. ± n.d.	0.28 ± 0.04	1.72 ± 0.23	1.38 ± 0.04	195	-0.596			
197.5	77.7	0.68	0.24 ± 0.09	0.19 ± 0.03	1.72 ± 0.08	0.58 ± 0.03	200	-1.132	0.1	1.06	76.6
207.5	82.0	0.71	0.28 ± 0.17	0.27 ± 0.06	1.89 ± 0.14	1.29 ± 0.03	210	-0.666	0.09	1.14	76.6

The third column shows the dry bulk density (DBD) in g/cm^3 as calculated from the water content following *Axelsson and Håkanson* [1971]. The error for the radionuclide measurements is 1 standard deviation of the mean. The $\delta^{18}O$ values of *N. dutertrei* are given in per mil relative to Pee Dee belemnite. Note that n.d. indicates not determined.

To a smaller extent, a decrease in deposition can also be seen at the 40- to 45-kyr mimimum where *Mazaud et al.* [1991] suggest a strongly increased production of ^{10}Be. This, however, may confirm the strength of the paleoproductivity maxima in stage 2 and at 40-45 kyr B.P. It should also be noted that although small changes in the concentration profiles of all radionuclide profiles occurred, the observed I_d minima are mainly caused by decreased ^{10}Be and $^{231}Pa_{ex}$ concentrations.

We summarize that the fluxes of the radionuclides ^{10}Be and ^{231}Pa to the sediments of the Galapagos microplate appear to be influenced by boundary-scavenging effects induced by paleoproductivity variations and corresponding changes in biogenic particle fluxes at the ocean margin areas of South America as, for example, are documented at the upwelling centers off Peru. These periods of enhanced boundary scavenging may have influenced the deposition of ^{10}Be and ^{231}Pa, although the sediments of our cores have been located under highly productive surface waters and thus an area of enhanced scavenging throughout the last 100 kyr.

This does not contradict results of *Lao et al.* [1992b] who did not find strongly increased I_d values of ^{10}Be and even found a decrease of the ^{231}Pa values in Peru margin sediments of the last glacial, because the missing amount of our radionuclides was not necessarily deposited exactly at the upwelling centers off the Peru margin. These authors proposed a more intense scavenging caused by increased particle fluxes throughout the ocean during glacials to explain their data. We also suggest that increased bioproductivity at the end of the last glacial period was not restricted to the upwelling centers off Peru, as for example, was also found by Y.-L. Yang et al. (Enhanced Uranium, excess ^{230}Th, and ^{231}Pa accumulation fluxes associated with the "carbon event" during the last glacial maximum in the Panama basin, submitted to *Paleocanography*, 1993), and that the area covered by highly productive surface waters was enlarged during glacial times. However, it probably did not cover all the Pacific Ocean [*Sarnthein and Winn*, 1990]. This may result in the same effect postulated by *Lao et al.* [1992b] that less ^{10}Be and possibly no ^{231}Pa of the amount missing in the Galapagos microplate cores could have reached the ocean margin off Peru.

Hydrothermal Activity

The Mn concentrations in the two investigated cores range from 0.02 to 0.47 wt % and the ones of Fe from 0.6 to 3.7 wt %. These values are low compared to hydrothermally influenced sediments from other areas, but they can be explained by high dilution with carbonate originating from the bioproductivity in the surface waters. The Mn/Fe ratio, however, is independent of dilution and thus serves to trace possible variations in the supply of hydrothermal Mn. In both cores the profiles of the Mn/Fe ratios show strong variations in a similar way: increased values mainly occur in the sections representing isotope stages 5 and 4, low ratios correspond to isotope stages 3 and 2, and a steep increase coincides with the beginning of isotope stage 1 (Figure 3).

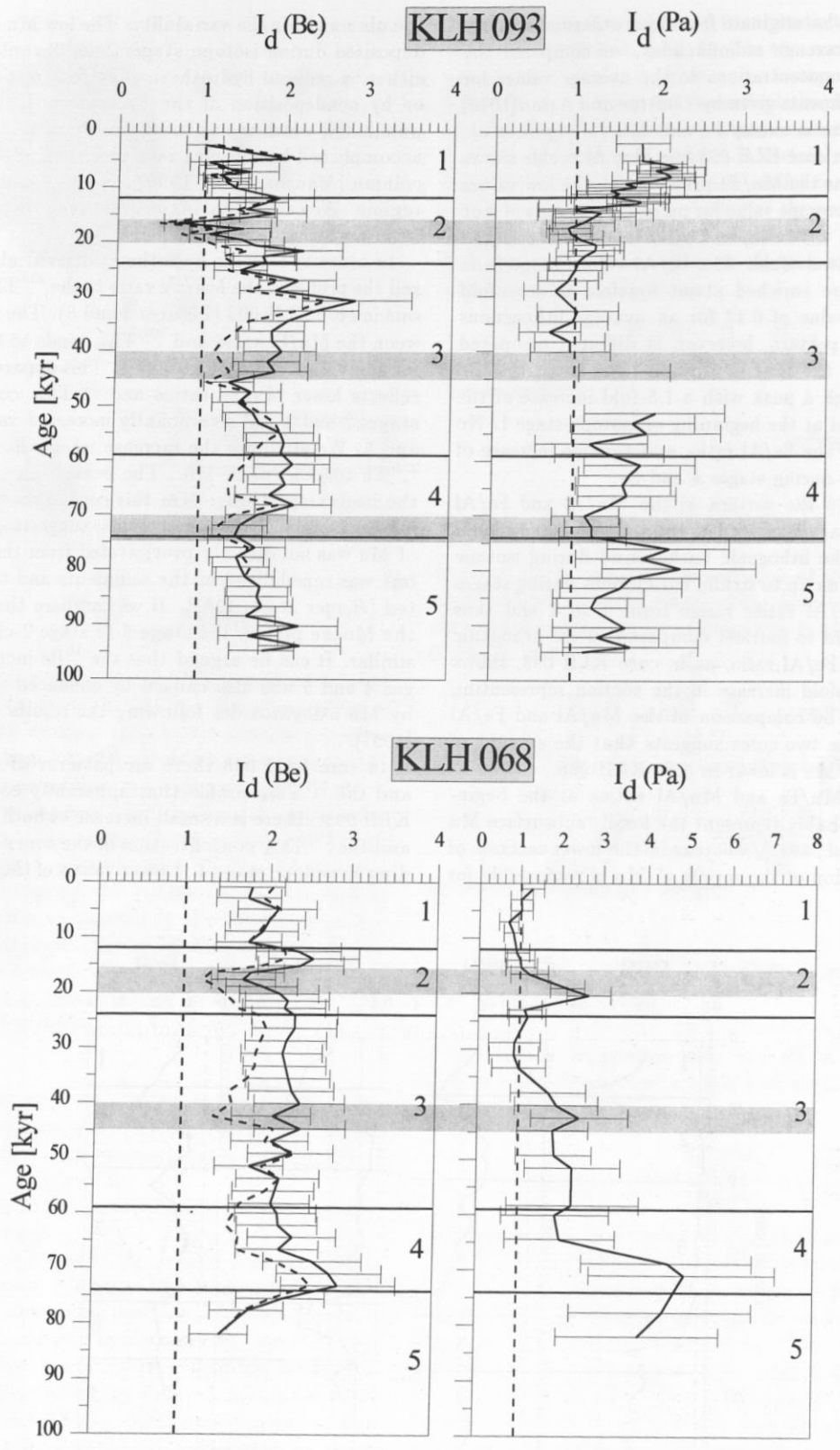

Figure 4. Deposition indices of ^{10}Be and ^{231}Pa versus age. The broken vertical lines mark depositon indices equal to 1. All values except the I_d(Be) values of core KLH 093 represent three-point running means of the calculated I_d values. The production rate corrected I_d(Be) profiles are plotted as a broken line. The transitions of the isotope stages are marked by horizontal lines. The shaded horizontal bars mark periods of enhanced paleoproductivity off Peru, as determined by *Oberhänsli et al.* [1990].

Because Fe may also originate from hydrothermal activity and is known to scavenge radionuclides, we compared the Fe/Al and Mn/Al concentrations to the average values for modern pelagic sediments given by *Chester and Aston* [1976] to check where there is excess Fe and Mn [*Mangini et al.*, 1993] (Figure 5). In core KLH 093 the Mn/Al profile shows the same patterns as the Mn/Fe profile, with the low values being equal to the average value for pelagic sediments of 0.06 and the increase in the isotope stages 1 and parts of 4 and 5 being sixfold to twelvefold. The Fe/Al values range from 2 to 3 and thus are enriched about fourfold to sevenfold compared to the value of 0.47 for an average lithogenous pelagic clay. The pattern, however, is different compared to the Mn/Fe and the Mn/Al profiles. The variations are only small, although a peak with a 1.5-fold increase of the Fe/Al ratio is found at the beginning of isotope stage 1. No relative increase of the Fe/Al ratio, and thus no increase of excess Fe occurred during stages 4 and 5.

In core KLH 068 the pattern of the Mn/Al and Fe/Al ratios is very similar. The Mn/Al ratio shows values equal to or lower than the lithogenic background during isotope stages 2 and 3 and an up to sixfold enrichment during stages 1 and 4. The Fe/Al ratios range from 1 to 2 and thus are enriched twofold to fourfold compared to the lithogenic background. The Fe/Al ratio, as in core KLH 093, shows a peak with a twofold increase in the section representing isotope stage 1. The comparison of the Mn/Al and Fe/Al ratio profiles of the two cores suggests that the amount of authigenic Fe and Mn is lower in core KLH 068.

The increased Mn/Fe and Mn/Al ratios at the beginning of stage 1 probably represent the fossil "subsurface Mn spike" [*Berger et al.*, 1983], whereas in the lower sections of the cores, fluctuation of the supply of Mn is responsible for the observed Mn/Fe variability. The low Mn concentrations deposited during isotope stages 2 and 3 could be explained either by reduced hydrothermal activity during these stages or by nondeposition of the hydrothermal Mn. The latter possibility, which seems to be more realistic, could either be accomplished by a longer residence time of Mn in the water column [*Mangini et al.*, 1990] or by a change in the current regime. We cannot distinguish between these two processes from our data.

In order to test the hypotheses derived above we compared the profile of the Mn/Fe ratio to the $^{230}Th_{ex}$ concentrations in core KLH 093 (Figures 3 and 6). The correlation between the Mn/Fe ratio and $^{230}Th_{ex}$ tends to be good, except for the values of isotope stage 1. This apparent relationship reflects lower Mn/Fe ratios and $^{230}Th_{ex}$ concentrations in stages 2 and 3 and significantly increased values in stages 4 and 5. We attribute the increase to enhanced deposition of ^{230}Th together with Mn. The peak of the Mn/Fe ratio at the beginning of stage 1 in this core is not accompanied by increased $^{230}Th_{ex}$ concentrations, suggesting that this peak of Mn was not directly precipitated from the water column, but was remobilized in the sediments and then reprecipitated [*Berger et al.*, 1983]. If we compare the ^{10}Be profile to the Mn/Fe profile, the stage 5 to stage 2 changes are quite similar. It can be argued that the ^{10}Be increase during stages 4 and 5 was also caused by enhanced scavenging of Be by Mn oxihydroxides following the results of *Bourlès et al.* [1991].

In core KLH 068 there are patterns of the Mn/Fe ratio and the $^{230}Th_{ex}$ profile that apparently correspond to core KLH 093. There is a small increase of both the Mn/Fe ratio and the $^{230}Th_{ex}$ concentration in the core section corresponding to isotope stage 4. Lower values of the Mn/Fe ratio du-

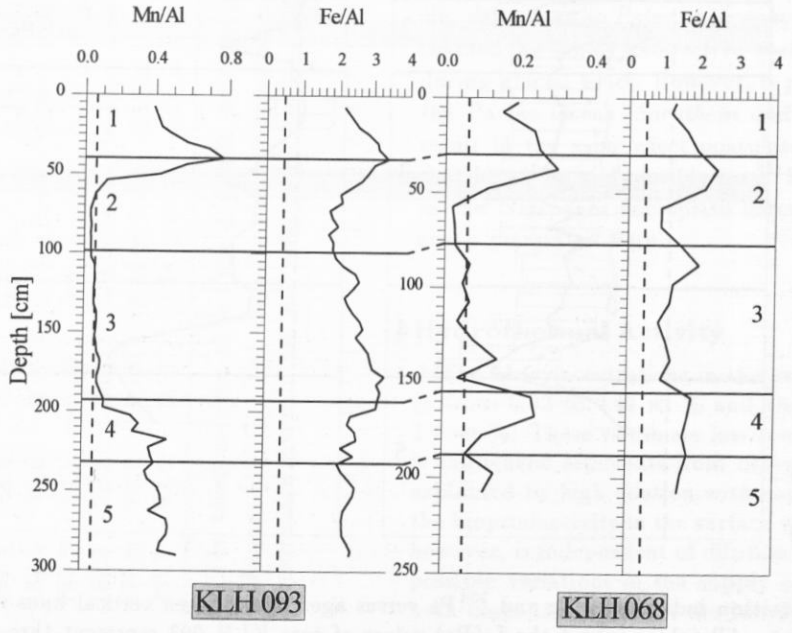

Figure 5. Profiles of the Mn/Al and Fe/Al ratios versus depth in core. The broken vertical lines mark the average ratios for pelagic sediments given by *Chester and Aston* [1976]. The transitions of the isotope stages are marked by horizontal lines.

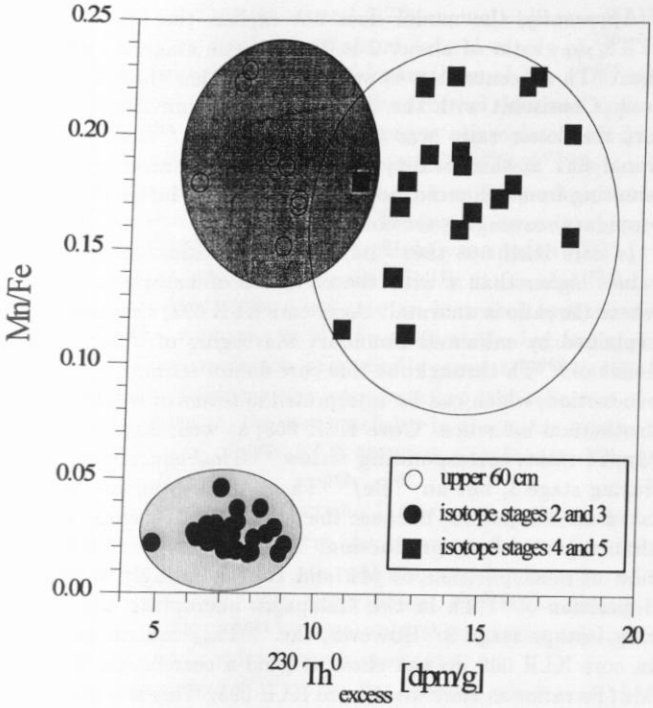

Figure 6. Correlation between the $^{230}Th_{ex}$ concentrations and the Mn/Fe ratios of core KLH 093. The upper 60 cm of the core are marked by open circles, the samples representing the isotope stages 2 and 3 are marked by solid circles, and the samples representing the isotope stages 4 and 5 are marked by solid squares. Three distinct amassments of points are visible: The upper 60 cm is characterized by high Mn/Fe ratios and relatively low $^{230}Th_{ex}$ concentrations (heavily shaded region); the samples of the core section between 60 and 195 cm are marked by low Mn/Fe ratios and low $^{230}Th_{ex}$ concentrations (lightly shaded region); and the samples of the core section lower than 195 cm are marked by high Mn/Fe ratios corresponding to high $^{230}Th_{ex}$ concentrations (unshaded region).

ring isotope stages 3 and 2 correspond to low $^{230}Th_{ex}$ concentrations during isotope stage 3. A weak increase of the $^{230}Th_{ex}$ concentration during isotope stage 1 corresdonds to a strongly increased Mn/Fe ratio.

Because the results of these comparisons are not unambigous, additional information on the influence of hydrothermalism on the deposition of ^{230}Th at this site was gathered from a model which compares the fluxes of ^{10}Be and ^{230}Th which exceed production normalized to the production ($^{10}Be/^{230}Th_{(F/P)}$ ratio). This model was presented by *Eisenhauer et al.* [1987] to trace paleoproductivity changes in the northwest Pacific Ocean (for detailed calculations see the work by *Eisenhauer* [1989]). Situations where the fluxes of the two radionuclides do not exceed production (e.g., oligotrophic central ocean gyres) are not described by the model. We assume that the total flux $F_{(x)}$ of either radionuclide to the sediment is

$$F_{(x)} = P + D \cdot \frac{dC_{(x)}}{dx} \tag{4}$$

where P is the flux expected from production, D is the eddy diffusion coefficient, and $C_{(x)}$ is the concentration of the nuclide at a distance x from an isotope sink where C is assumed to be 0 for mathematical simplification. This is simplified and a first-order approximation, because $C_{(x)}$ in a center of biological activity is certainly lowered but not equal to 0. Nevertheless, the model is able to deliver a qualitatively correct description of the scavenging behavior of radionuclides in an area of enhanced scavenging. The flux then can be normalized to the flux of the radionuclide expected from production:

$$\frac{F - P}{P} = \frac{D}{P} \cdot \frac{dC_{(x)}}{dx} \tag{5}$$

Assuming then

$$C_{(x)} = C_0 \cdot \left(1 - e^{-\frac{x}{\sqrt{D \cdot \Theta}}}\right) \tag{6}$$

$$P = \frac{C_0 \cdot h}{\Theta} \tag{7}$$

where C_0 is the initial concentration of the nuclide in the water column, h is the height of the water column, and Θ is the residence time of the radionuclide in the water column, it follows that

$$\frac{F - P}{P} = \frac{\sqrt{D \cdot \Theta}}{h} \cdot e^{-\frac{x}{\sqrt{D \cdot \Theta}}} \tag{8}$$

The $^{10}Be/^{230}Th_{ex(F/P)}$ ratio can then be defined as

$$\frac{^{10}Be}{^{230}Th_{(F/P)}} = \frac{\frac{F_{Be} - P_{Be}}{P_{Be}}}{\frac{F_{Th} - P_{Th}}{P_{Th}}} \tag{9}$$

By inserting equation 8 we get

$$\frac{\frac{F_{Be} - P_{Be}}{P_{Be}}}{\frac{F_{Th} - P_{Th}}{P_{Th}}} = \frac{\sqrt{\Theta_{Be}}}{\sqrt{\Theta_{Th}}} \cdot e^{x \cdot \left(\frac{1}{\sqrt{D \cdot \Theta_{Th}}} - \frac{1}{\sqrt{D \cdot \Theta_{Be}}}\right)} \tag{10}$$

At a center of an isotope sink (x = 0), such as the highly productive divergence zone of two surface currents, we calculate

$$\frac{^{10}Be}{^{230}Th_{(F/P)}} = \frac{\frac{F_{Be} - P_{Be}}{P_{Be}}}{\frac{F_{Th} - P_{Th}}{P_{Th}}} = \sqrt{\frac{\Theta_{Be}}{\Theta_{Th}}} \tag{11}$$

This means that at a center of biological productivity, the $^{10}Be/^{230}Th_{(F/P)}$ ratio in the sediments should only be dependent on the square root of the residence times of the two radionuclides. Assuming a mean residence time of about 25 years for ^{230}Th and of 400 years for ^{10}Be (which is at the lower end of the evaluations of the mean residence time values in literature), the $^{10}Be/^{230}Th_{(F/P)}$ ratio should then amount to about 4. This value was already observed by *Mangini et al.* [1984] in sediments from the upwelling centers off West Africa and the circumpolar divergence zone. At a certain distance from the center of biological activity the ratio then increases because the ^{10}Be can be supplied horizontally from a much larger area than ^{230}Th. The water column concentrations at a distance from the isotope sink therefore will still be enriched in ^{10}Be compared to ^{230}Th.

The $^{10}Be/^{230}Th_{(F/P)}$ ratios lower than 4, which were named Th anomalies, are only possible if a selective scavenging of ^{230}Th occurs that does not enhance the ^{10}Be scavenging to the same extent. These Th anomalies, for example, have been observed at glacial/interglacial transitions in sediment cores where the fluxes of both isotopes exceeded production and were ascribed to enhanced bottom water oxygenation and a precipitation of dissolved Mn, which scavenged the ^{230}Th from the water column [*Eisenhauer et al.*, 1990; *Mangini et al.*, 1990].

We expect these Th anomalies to occur in hydrothermally influenced sediments as well. Following the model presented above, $^{10}Be/^{230}Th_{(F/P)}$ ratios lower than 4 are predicted in core sections representing periods of enhanced scavenging of ^{230}Th. The $^{10}Be/^{230}Th_{(F/P)}$ ratios for each climatic stage of the two cores are shown in Figure 7. The broken line plot represents the lower production rate corrected values following *Mazaud et al.* [1991]. The contrast between the high ratios in stage 3 and the low ones in stages 2 and 4, however, remains the same. In core KLH 093, the $^{10}Be/^{230}Th_{(F/P)}$ ratios are significantly lower than 4 throughout the core (average below 2) except during stage 3. The ratios lower than 4 in the core sections corresponding to the isotope stages 4 and 5 may be explained by enhanced deposition of ^{230}Th. The data suggest that the low $^{10}Be/^{230}Th_{(F/P)}$ ratio of climatic stage 1 results from a slightly higher deposition of ^{230}Th combined with a slightly decreased deposition of ^{10}Be. The $^{10}Be/^{230}Th_{(F/P)}$ value of 5 (e.g., 4 production rate corrected) in the isotope stage 3 corresponds to the observed lowered deposition of ^{230}Th and Mn in this section.

Apparently, the model does not explain the low $^{10}Be/^{230}Th_{(F/P)}$ ratio of about 2 in the climatic stage 2, where the ^{230}Th concentration is only slightly higher than in stage 3. Consistent with the discussion in the previous chapter, this lower ratio was caused by a lower ^{10}Be depositional flux at this locality during most of isotope stage 2 resulting from enhanced boundary-scavenging intensity (see boundary-scavenging section).

In core KLH 068 the $^{10}Be/^{230}Th_{(F/P)}$ ratios amount to values higher than 4 with the exception of isotope stage 2, where the ratio is anormal. As in core KLH 093, this may be explained by enhanced boundary scavenging of ^{10}Be. The fluxes of ^{230}Th throughout this core do not strongly exceed production, which can be interpreted in terms of weaker hydrothermal influence. Core KLH 068, as well, displays low Mn/Fe ratios corresponding to low $^{230}Th_{ex}$ concentrations during stage 3, but no $^{10}Be/^{230}Th_{(F/P)}$ ratio can be calculated for this period, because the fluxes of ^{230}Th were lower than expected from production. This supports the assumption of nondeposition of Mn and correspondingly lowered deposition of ^{230}Th in the Galapagos microplate area during isotope stage 3. However, the $^{230}Th_{ex}$ concentrations in core KLH 068 do not show as good a correlation to the Mn/Fe ratios as they do in core KLH 093. This is probably the result of various short-term dilution events with basaltic glass, for example, around 120 cm core depth. The source of these disturbances is the seamount mentioned before, which is located in the neighbourhood of the KLH 068 core site (see Figure 1). For this reason, the results derived from core KLH 093 are considered more reliable.

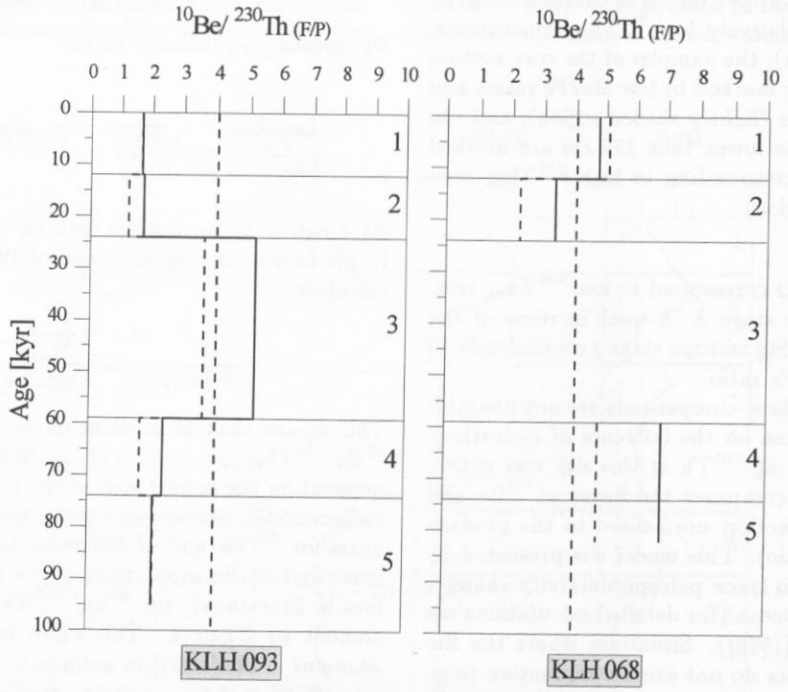

Figure 7. The $^{10}Be/^{230}Th_{(F/P)}$ ratios of core KLH 068 and 093 versus depth in core. The production rate corrected $^{10}Be/^{230}Th_{(F/P)}$ ratios are plotted as a broken line. The transitions of the isotope stages are marked by horizontal lines. The broken vertical lines mark a $^{10}Be/^{230}Th_{(F/P)}$ ratio of 4. For the isotope stage 3 in core KLH 068, no $^{10}Be/^{230}Th_{(F/P)}$ ratio could be calculated, because the ^{230}Th fluxes did not exceed production.

We conclude that the stage 4-5 Th anomalies in core KLH 093 may be the result of enhanced lateral supply of ^{230}Th caused by enhanced supply of hydrothermal Mn. During isotope stages 3 and 2, the hydrothermal Mn was apparently not deposited in the Galapagos microplate area for reasons we can only speculate about. The ^{10}Be/^{230}Th$_{(F/P)}$ ratios below 4 during isotope stage 2 in both cores were probably caused by enhanced ^{10}Be boundary scavenging. In core KLH 093 during stage 1, slightly increased ^{230}Th$_{ex}$ concentrations, strongly increased Mn/Fe ratios, and ^{10}Be/^{230}Th$_{(F/P)}$ ratios below 4 indicate an increased hydrothermal influence, whereas the Mn/Fe peak at the beginning of stage 1 in both cores was presumably caused by remobilization of Mn. Following our interpretation, the influence of hydrothermalism on the radionuclides in the water column overlying the site of core KLH 068 was significantly lower than at core KLH 093.

Here we have to note that the I_d(Be) and I_d(Pa) values of core KLH 093 calculated in the previous chapter for the isotope stages 5, 4, and 1 are probably too low because of the lateral supply of ^{230}Th. Nevertheless, the results derived in this section are valid, because only short-lasting relative decreases of the I_d values were investigated.

The calculation of ^{230}Th$_{ex}$/^{231}Pa$_{ex}$ ratios, which may also serve as a tool to determine hydrothermal activity, is not as reliable as the results above because of the high statistical uncertainties of the ^{231}Pa measurement. Nevertheless, average ratios of about 6 in core KLH 093 also suggest a strong scavenging of both radionuclides that may have been caused by hydrothermal influence. The downcore variations of the ^{230}Th$_{ex}$/^{231}Pa$_{ex}$ ratios do not show a strong relationship to the interpretations above. A slight decrease of the ^{230}Th$_{ex}$/^{231}Pa$_{ex}$ during stage 1 and roughly during stages 4 and 5 in core KLH 093 tends to confirm the periods of hydrothermal activity determined above. We argue, however, that the effect of increased biological particle fluxes from highly productive surface waters, as discussed in the previous section left a stronger imprint on the ^{230}Th$_{ex}$/^{231}Pa$_{ex}$ ratios than hydrothermal activity in our cores. In Table 3 the results of the discussion are summarized.

Conclusions

The scavenging processes in the water column of the Galapagos microplate area have been influenced by three main factors throughout the last 100 kyr: changes in surface water productivity, boundary scavenging, and hydrothermal influence. The importance and the variations of these factors through time were evaluated by high-resolution measurements of the radionuclides ^{10}Be, ^{230}Th, and ^{231}Pa and, additionally, Mn and Fe in the underlying sediments.

Fluctuations of the deposition indices of ^{10}Be and ^{231}Pa probably reflect effects of varying boundary-scavenging intensity caused by paleoproductivity changes; our results suggest that these fluctuations are connected to changes in biogenic particle fluxes at the ocean margin and an enlargement of the equatorial high-productivity zone, for example, in the last glacial. Maxima in paleoproductivity as determined in sediments from off Peru appear to coincide with

Table 3. Summary of Major Points

Observation	Time Interval in the Investigated cores	Interpretation
I_d(Be) and I_d(Pa) > 1	most parts of both cores	Enhanced scavenging of ^{10}Be and ^{231}Pa caused by high surface water productivity above the core sites
Minima of I_d(Be) and I_d(Pa) apparently coincide with paleoproductivity maxima at the upwelling centers off Peru	KLH 093: around 18, 45, and 72 kyr B.P., I_d(Pa) around 18 and 72kyr B.P.; KLH 068: I_d(Be)	Periods of enhanced boundary scavenging of ^{10}Be and ^{231}Pa
^{10}Be/^{230}Th$_{(F/P)}$ ratios < 4 correspond to low Mn and ^{230}Th$_{ex}$ concentrations	KLH 093 and KLH 068: isotope stage 2	Enhanced boundary scavenging of ^{10}Be
^{10}Be/^{230}Th$_{(F/P)}$ ratios < 4 correspond to increased ^{230}Th$_{ex}$ and Mn concentrations	KLH 093: isotope stages 4 and 5	Enhanced deposition of hydrothermal Mn
Increased Mn concentrations do not correspond to increased ^{230}Th$_{ex}$ concentrations	KLH 093: beginning of isotope stage 1 in the sediment	Mn remobilization and reprecipitation

Observations in the studied cores KLH 093 and KLH 068, Galapagos microplate, and the time intervals of their occurrence are shown in columns 1 and 2. In column 3 the corresponding interpretations are listed.

minima of ^{231}Pa and ^{10}Be deposition in the Galapagos microplate sediments. This suggests that ^{10}Be and to a lesser extent ^{231}Pa have been sensitive to changes in paleoproductivity and particle fluxes at the ocean margin, although highly productive surface waters were situated above the core sites throughout the last 30 kyr and probably also the last 100 kyr.

The $^{10}Be/^{230}Th_{(F/P)}$ ratios < 4 indicate enhanced ^{230}Th scavenging in core KLH 093 throughout most of the last 100 kyr except stage 3. Core KLH 068, which was not deposited under comparably undisturbed conditions, reveals $^{10}Be/^{230}Th_{(F/P)}$ ratios around 4 or higher throughout the last 85 kyr except stages 2 and 3. The $^{10}Be/^{230}Th_{(F/P)}$ ratios representing isotope stage 3 in both cores indicate a period of "normal" ^{230}Th scavenging that coincides with a decreased Mn deposition. For this decrease that could as well be interpreted as a consequence of a diminished hydrothermal supply of Mn, we propose a climatically controlled change of the current regime or a decrease in bottom water oxygenation that led to nondeposition of Mn in the Galapagos microplate area. The stage 2 Th anomaly in both cores can be ascribed to a diminished ^{10}Be flux to the sediments caused by enhanced boundary scavenging intensity.

The $^{10}Be/^{230}Th_{(F/P)}$ ratios < 4 which apparently correlate to increased Mn and $^{230}Th_{ex}$ concentrations may serve as a tool to evaluate enhanced hydrothermal influence on deep-sea sediments as is the case in core KLH 093 in the core sections representing isotope stages 5 and 4 and to a lesser extent during stage 1. In these core sections the I_d values of the boundary-scavenging model were calculated too low because of the lateral transport of ^{230}Th, but the conclusions derived above are nevertheless valid. The Mn/Fe peak at the beginning of stage 1 that does not coincide with similarly increased $^{230}Th_{ex}$ concentrations in both cores probably is less the result of primary deposition of hydrothermal Mn from the water column than of mainly remobilization and reprecipitation of this element during isotope stage 2. This process terminated at the transition from isotope stage 2 to 1 and then restarted with lower intensity.

The application of the two models presented here does not reveal contradictory results but helps to distinguish between different particle flux processes, for example, hydrothermal activity, high biological productivity of the surface waters, and boundary scavenging processes, all of which affect the accumulation of ^{10}Be, ^{230}Th, and ^{231}Pa in the Galapagos microplate sediments.

Acknowledgments. This study was supported by the BMFT, project HYMAS II, PLR/2/HEL 03R391D9. We thank R.F. Anderson, Lamont Doherty Earth Observatory, Palisades, New York, and an anonymus reviewer for helpful comments and discussion. We like to thank T. Alt and R. Walther, Heidelberger Akademie der Wissenschaften, for the ESR measurements and H.-W. Hubberten and G. Meyer, Alfred Wegener Institut für Polar- und Meeresforschung, Bremerhaven, for the δ^{18}O measurements of core KLH 068. We thank H. Puchelt, Institut für Petrographie und Geochemie, Karlsruhe, for ship time and providing samples.

References

Anderson, R. F., M. P. Bacon, and P. G. Brewer, Removal of ^{230}Th and ^{231}Pa from the open ocean, *Earth Planet. Sci. Lett., 62*, 7-23, 1983a.

Anderson, R. F., M. P. Bacon, and P. G. Brewer, Removal of ^{230}Th and ^{231}Pa at ocean margins, *Earth Planet. Sci. Lett., 66*, 73-90, 1983b.

Anderson, R. F., Y. Lao, W. S. Broecker, S. E. Trumbore, H. J. Hofmann, and W. Wölfli, Boundary scavenging in the Pacific Ocean: A comparison of ^{10}Be and ^{231}Pa, *Earth Planet. Sci. Lett., 96*, 287-304, 1990.

Axelsson, V., and L. Håkanson, Sambandet mellan kvicksilverförekomst och sedimentologisk miljö i Ekoln. Del 1. Målsättning och analysmetodik, *UNGI Rap 11*, 35 pp., Univ. Uppsala, Uppsala, 1971.

Bacon, M. P., and R. F. Anderson, Distribution of thorium isotopes between dissolved and particulate forms in the deep sea, *J. Geophys. Res., 87*(C3), 2045-2056, 1982.

Berger, W. H., R. C. Finkel, J. S. Killingley, and V. Marchig, Glacial-Holocene transition in deep-sea sediments: Manganese-spike in the East-Equatorial Pacific, *Nature, 303*, 231-233, 1983.

Bourlès, D. L., G. M. Raisbeck, and F. Yiou, ^{10}Be and ^{9}Be in marine sediments and their potential for dating, *Geochim. Cosmochim. Acta, 53*, 443-452, 1989a.

Bourlès, D. L., G. Klinkhammer, A. C. Campbell, C. I. Measures, E. T. Brown, and J. M. Edmond, Beryllium in marine pore waters: Geochemical and geochronological implications, *Nature, 341*, 731-733, 1989b.

Bourlès, D. L., G. M. Raisbeck, E. T. Brown, F. Yiou, and J. M. Edmond, Beryllium isotope systematics of submarine hydrothermal sediments, *Earth Planet. Sci. Lett., 105*, 534-542, 1991.

Brown, E. T., C. I. Measures, J. M. Edmond, D. L. Bourlès, G. M. Raisbeck and F. Yiou, Continental inputs of beryllium to the oceans, *Earth Planet. Sci. Lett., 114*, 101-111, 1992.

Chester, R., and S. R. Aston, The geochemistry of deep-sea sediments, in *Chemical Oceanography*, 2nd ed. vol. 6, edited by J. P. Riley and R. Chester, chapter 34, Academic, San Diego, Calif., 1976.

Eckhardt, J.-D., Geochemische Untersuchungen an jungen Sedimenten von der Galapagos-Mikroplatte: hydrothermale und stratigraphisch signifikante Signale, *Karlsruher Geochem. Hefte, 3*, 1-157, 1992.

Eisenhauer, A., ^{10}Be und ^{230}Th: Eine Zwei Tracer Studie mariner Sedimente, Ph.D. thesis, Univ. Heidelberg, Heidelberg, Germany, 1989.

Eisenhauer, A., A. Mangini, M. Segl, J. Beer, G. Bonani, M. Suter and W. Wölfli, High resolution ^{10}Be and ^{230}Th profiles in DSDP site 580, *Nucl. Instrum. Methods Phys. Res., B29*, 326-331, 1987.

Eisenhauer, A., A. Mangini, R. Botz, P. Walter, J. Beer, G. Bonani, H. J. Hofmann, M. Suter, and W. Wölfli, High resolution ^{10}Be and ^{230}Th stratigraphy of late Quaternary sediments from the Fram Strait (core 23235), in *Geological History of the Polar Oceans: Arctic versus Antarctic*, edited by U. Bleil and J. Thiede, pp. 475-487, Kluwer Academic, Norwell, Mass., 1990.

Eisenhauer, A., K. Gögen, E. Pernicka, and A. Mangini, Climatic influences on the growth rates of Mn crusts during the late Quaternary, *Earth Planet. Sci. Lett., 109*, 25-36, 1992.

Henken-Mellies, W. U., J. Beer, F. Heller, K. J. Hsü, C. Shen, G. Bonani, H. J. Hofmann, M. Suter, and W. Wölfli, ^{10}Be and ^{9}Be in South Atlantic DSDP site 519: Relation to geomagnetic reversals and to sediment composition, *Earth Planet. Sci. Lett., 98*, 267-276, 1990.

Hofmann, H. J., J. Beer, G. Bonani, H. R. von Gunten, S. Raman, M. Suter, R. L. Walker, W. Wölfli and D. Zimmermann, ^{10}Be: Half-life and AMS-standards, *Nucl. Instrum. Methods Phys. Res., B29*, 2-36, 1987.

Imbrie, J., J. D. Hays, D. G. Martinson, A. Mc Intyre, A. C. Mix, J. J. Morley, N. G. Pisias, W. L. Prell, and N.J. Shackleton, The orbital theory of Pleistocene climate: Support from a revised chronology of the marine δ^{18}O record, in *Milankovitch and Climate, Part I*, edited by A. L. Berger et al., pp. 269-305, D. Reidel, Norwell, Mass., 1984.

Ivanovich, M., and R. S. Harmon (Eds.), *Uranium Series Disequilibrium*, 2nd ed., 910 pp., Clarendon, Oxford, 1992.

Jansen, J. H. F., C. Alderliesten, A. J. van Bennekom, K. van der Borg, and A. F. M. De Jong, Terrigenous supply of ^{10}Be and dating with ^{14}C and ^{10}Be in sediments of the Angola Basin (SE Atlantic), *Nucl. Instrum. Methods Phys. Res., B29*, 311-316, 1987.

Ku, T. L., L. Kusakabe, C. I. Measures, J. R. Southon, J. S. Vogel, D. E. Nelson, and S. Nakaya, Be isotope distribution in the western North Atlantic: A comparison to the Pacific, *Deep Sea Res., 37*, 795-808, 1990.

Kusakabe, L., T. L. Ku, J. R. Southon, J. S. Vogel, D. E. Nelson, C. I. Measures, and Y. Nozaki, The distribution of ^{10}Be and ^{9}Be in ocean water, *Nucl. Instrum. Methods Phys. Res., B29*, 306-310, 1987.

Kusakabe, L., T. L. Ku, J. R. Southon, S. Liu, J. S. Vogel, D. E. Nelson, S. Nakaya, and G. L. Cusinmano, Be isotopes in rivers/estuaries and their oceanic budgets, *Earth Planet. Sci. Lett., 102*, 265-276, 1991.

Lal, D., and B. Peters, Cosmic ray produced radioactivity on the Earth, in *Encyclopedia of Physics 46*(2), pp. 581-588, Springer-Verlag, New York, 1967.

Lao, Y., Transport and burial rates of ^{10}Be and ^{231}Pa in the Pacific Ocean, Ph.D. thesis, Columbia Univ., New York, 1991.

Lao, Y., R. F. Anderson, W. S. Broecker, S. E. Trumbore, H. J. Hofmann, and W. Wölfli, Increased production of cosmogenic ^{10}Be during the last glacial maximum, *Nature, 357*, 576-578, 1992a.

Lao, Y., R. F. Anderson, and W. S. Broecker, Boundary scavenging and deep-sea sediment dating: Constraints from excess ^{230}Th and ^{231}Pa, *Paleoceanography, 7*, 783-798, 1992b.

Lao, Y., R. F. Anderson, W. S. Broecker, S. E. Trumbore, H. J. Hofmann, and W. Wölfli, Transport and burial rates of ^{10}Be and ^{231}Pa in the Pacific ocean during the Holocene period, *Earth Planet. Sci. Lett., 113*, 173-189, 1992c.

Lao, Y., R. F. Anderson, W. S. Broecker, H. J. Hofmann, and W. Wölfli, Particulate fluxes of ^{230}Th, ^{231}Pa and ^{10}Be in the northeastern Pacific Ocean, *Geochim. Cosmochim. Acta, 57*, 205-217, 1993.

Lonsdale, P., Structural pattern of the Galapagos microplate and evolution of the Galapagos triple junctions, *J. Geophys. Res., 93*(B11), 13,551-13,574, 1988.

Mangini, A., and L. Diester-Haass, Excess ^{230}Th in N.W. African sediments traces upwelling in the past, in *Coastal Upwelling: Its Sediment Record* edited by E. Suess and J. Thiede, *NATO Conf. Ser., Ser. IV, 10a*, 455-470, 1983.

Mangini, A., and C. Sonntag, ^{231}Pa dating of deep-sea cores via ^{227}Th counting, *Earth Planet. Sci. Lett., 37*, 251-256, 1977.

Mangini, A., C. Sonntag, G. Bertsch, and E. Müller, Evidence for a higher, natural U-content in world rivers, *Nature, 79*, 337-339, 1979.

Mangini, A., M. Segl, G. Bonani, H. J. Hofmann, E. Morenzoni, M. Nessi, M. Suter, W. Wölfli, and K. K. Turekian, Mass spectrometric ^{10}beryllium dating of deep sea sediments applying the Zürich tandem accelerator, *Nucl. Instrum. Methods Phys. Res., B5*, 353-357, 1984.

Mangini, A., A. Eisenhauer, and P. Walter, Response of Mn in the ocean to the climatic cycles in the Quaternary, *Paleoceanography, 5*, 811-821, 1990.

Mangini, A., H.-J. Rutsch, M. Frank, A. Eisenhauer, J.-D. Eckhardt, Is there a relationship between atmospheric CO_2 and manganese in the ocean, in *Carbon Cycling in the Glacial Ocean: Constraints on the Ocean's Role in Global Change*, edited by R. Zahn et al., *NATO ASI Ser., Ser. I, 17*, 87-104, 1993.

Martinson, D. G., N. G. Pisias, J. D. Hays, J. Imbrie, T. C. Moore Jr., and N.J. Shackleton, Age dating and the orbital theory of the ice ages: Development of a high-resolution 0 to 300,000-year chronostratigraphy, *Quat. Res., 27*, 1-29, 1987.

Mazaud, A., C. Laj, E. Bard, M. Arnold, and E. Tric, Geomagnetic field control of ^{14}C production over the last 80 ky: Implications for the radiocarbon time-scale, *Geophys. Res. Lett., 18*(10), 1885-1888, 1991.

Monaghan, M., S. Krishnaswami, and K. K. Turekian, The global-average production rate of ^{10}Be, *Earth Planet. Sci. Lett., 76*, 279-287, 1985/1986.

Mudelsee, M., M. Barabas, and A. Mangini, ESR dating of the Quaternary deep-sea sediment core RC17-177, *Quat. Sci. Rev., 11*, 181-189, 1991.

Nozaki, Y., Y. Horibe, and H. Tsubota, The water column distributions of thorium isotopes in the western North Pacific, *Earth Planet. Sci. Lett., 54*, 203-216, 1981.

Oberhänsli, H., P. Heinze, L. Diester-Haass, and G. Wefer, Upwelling off Peru during the last 430,000 yr and its relationship to the bottom-water environment, as deduced from coarse grain-size distributions and analyses of benthic foraminifers at holes 679D, 680B and 681B, Leg. 112, in *Proc. Ocean Drill. Program Sci. Res., 112*, 369-390, 1990.

Sarnthein, M., and K. Winn, Reconstruction of low and middle latitude export productivity, 30,000 years BP to present: Implications for global carbon reservoirs, in *Climate-Ocean Interaction*, edited by M.E. Schlesinger, pp. 319-342, Kluwer Academic, Norwell, Mass., 1990.

Segl, M., A. Mangini, J. Beer, G. Bonani, M. Suter, W. Wölfli, and C. Measures, ^{10}Be in the Atlantic Ocean, a transect at 25°N, *Nucl. Instrum. Methods Phys. Res., B5*, 332-334, 1987.

Sharma, P., P. Mahannah, W. S. Moore, T. L. Ku, and J. R. Southon, Transport of ^{10}Be and ^{9}Be in the ocean, *Earth Planet. Sci. Lett., 86*, 69-76, 1987.

Shimmield, G. B., and N. B. Price, The scavenging of U, ^{230}Th and ^{231}Pa during pulsed hydrothermal activity at 20°S, East Pacific Rise, *Geochim. Cosmochim. Acta, 52*, 669-677, 1988.

Southon, J. R., T. L. Ku, D. E. Nelson, J. L. Reyss, J. C. Duplessy, and J. S. Vogel, ^{10}Be in a deep-sea core: Implications regarding ^{10}Be production changes over the past 420 ka, *Earth Planet. Sci. Lett., 85*, 356-364, 1987.

Turekian, K. K., L. K. Benneinger, and E. P. Dion, ^{7}Be and ^{210}Pb total depositional fluxes at New Haven, Connecticut, and at Bermuda, *J. Geophys. Res., 88* (C9), 5411-5415, 1983.

Valette-Silver, J. N., F. Tera, J. Klein, and R. Middleton, Beryllium 10 in hydrothermal vent deposits from the east Pacific ridges: Role of sediments in the hydrothermal processes, *J. Geophys. Res., 92*(B11), 11,364-11,372, 1987.

Winograd, I. J., T. B. Coplen, J. M. Landwehr, A. C Riggs, K. R. Ludwig, B. J. Szabo, P. T. Kolesar, and K. M. Revesz, Continous 500,000-year climate record from vein calcite in Devil's Hole, Nevada, *Science, 258*, 255-260, 1992.

Yang, H.-S., Y. Nozaki, Y. Sakai, and A. Masuda, The distribution of ^{230}Th and ^{231}Pa in the deep surface sediments of the Pacific Ocean, *Geochim. Cosmochim. Acta, 50*, 2499-2507, 1986.

B. Dittrich-Hannen and P.W. Kubik, Institut für Teilchenphysik der ETH Zürich, ETH-Hönggerberg, CH-8093 Zürich, Switzerland. (e-mail: dittrich@imp.phys.ethz.ch; kubik@czheth5a)

J.-D. Eckhardt, Institut für Petrographie und Geochemie, Universität Karlsruhe, Kaiserstrasse 12, 76131 Karlsruhe, Germany.

A. Eisenhauer, M. Frank, and A. Mangini, Heidelberger Akademie der Wissenschaften, INF 366, 69120 Heidelberg, Germany. (e-mail: Ei@uphys1.uphysn.uni-heidelberg.de; Fk@uphys1.uphysn.uni-heidelberg.de; Mg@uphys1.uphysn.uni-heidelberg.de)

M. Segl, Fachbereich Geowissenschaften, Universität Bremen, Postfach 330 440, 28334 Bremen, Germany.

(Received August 18, 1993; revised April 22, 1994; accepted April 26, 1994.)